2023 COASTAL MASTER PLAN

ICM-WETLANDS – SUBMERGED AQUATIC VEGETATION (SAV) UPDATES

ATTACHMENT D3

REPORT: VERSION 02
DATE: JULY 2023
PREPARED BY: KRISTIN DEMARCO, DONALD SCHOOLMASTER, BRADY COUVILLION

COASTAL PROTECTION AND RESTORATION AUTHORITY

This document was developed in support of the 2023 Coastal Master Plan being prepared by the Coastal Protection and Restoration Authority (CPRA). CPRA was established by the Louisiana Legislature in response to Hurricanes Katrina and Rita through Act 8 of the First Extraordinary Session of 2005. Act 8 of the First Extraordinary Session of 2005 expanded the membership, duties, and responsibilities of CPRA and charged the new authority to develop and implement a comprehensive coastal protection plan, consisting of a master plan (revised every six years) and annual plans. CPRA's mandate is to develop, implement, and enforce a comprehensive coastal protection and restoration master plan.

CITATION

DeMarco, K., Schoolmaster, D., Couvillion, B. R. (2023). 2023 Coastal Master Plan: Attachment D3: ICM-Wetlands – Submerged Aquatic Vegetation (SAV) Updates. Version 02. (pp. 1-58). Baton Rouge, Louisiana: Coastal Protection and Restoration Authority.

ACKNOWLEDGEMENTS

EXECUTIVE SUMMARY

Submerged aquatic vegetation (SAV) provides critical structural habitat for valuable nekton and wildlife species across coastal ecosystems and can buffer the negative effects of land loss. Landscape change and restoration efforts across coastal Louisiana can impact the occurrence, coverage, and species assemblages of SAV, and changes to these foundational species can have cascading impacts across food webs. To support the 2023 Coastal Master Plan efforts, a unique SAV model was developed to assess coverage and occurrence of SAV across aquatic waterbodies in response to environmental variables evaluated.

This effort created a spatial model describing the probability of presence of SAV across the study area in response to changing conditions over the modeled time period. To develop the initial coverage data layer, we used remotely sensed Normalized Difference Vegetation Index (NDVI) and modified Normalized Difference Water Index (mNDWI) data from 2015-2018 to identify areas containing variable vegetation and water spectral reflectance. Key environmental variables evaluated included total suspended sediments (TSS), salinity, and physical exposure. Seasonal estimates for TSS and salinity were used, as research indicates that seasonal environmental variability is a significant driver for SAV establishment. Seasonal salinity was derived from Coast-wide Reference Monitoring Station (CRMS) data, and seasonal TSS was estimated from hyperspectral imagery. Estimates of physical exposure have previously been provided by calculating fetch (the distance across water over which waves can propagate), but this proved to be too computationally intensive to be feasible, and we found distance to land to be a reasonable proxy for exposure. To represent geographic conditions and historical factors influences on SAV establishment and occurrence (e.g., variables too numerous and complex to model) we developed a basin variable that served as a proxy for complex historical, or prior, conditions, determined by the forested, fresh, intermediate, brackish, or saline (FFIBS) score. The final model included spring TSS, spring salinity, distance to land, and the basin prior.

The model performed well for the area evaluated, correctly classifying SAV (as present or absent) 89% of the time (Kappa = 580). SAV probability of presence responded as expected to change in these environmental variables, with likelihood of occurrence decreasing in response to increasing spring TSS, spring salinity, and distance to land. However, the model was more accurate at predicting absence (true negative = 0.940) than predicting presence (true positive = 0.626), suggesting that the scale of the model may limit the ability to predict presence. Moreover, the simplicity of the model limited the accuracy in highly dynamic environments, for example near the outflow of diversions or areas of significant changes in salinity or TSS.

Through incorporating underwater communities like SAV, this master plan provides a holistic view of coastal change and restoration. To create healthy ecological structure and function in wetland habitats, the submergent communities must be considered alongside the emergent habitats. As the benefits of SAV are increasingly recognized, both here in Louisiana and beyond, SAV restoration and the use of SAV communities in assessing and improving ecological condition are becoming more common.

TABLE OF CONTENTS

LIST OF TABLES

LIST OF FIGURES AND EQUATIONS

LIST OF ABBREVIATIONS

1.0 INTRODUCTION

To support the 2023 Coastal Master Plan efforts, a unique submerged aquatic vegetation (SAV) model was developed to assess coverage across aquatic waterbodies. The presence, cover, and species assemblages of SAV across coastal ecosystems is a critical component to understanding landscape scale response to changes in environmental conditions and restoration efforts. SAV provides significant ecosystem services in coastal systems, acting as a foundational species and ecological engineer, where healthy SAV beds create essential habitat for valuable nekton and wildlife species, improve water quality, and reduce coastal erosion (Gracia et al., 2017; Juston et al., 2013; Västilä and Järvelä, 2017; Yan et al., 2016). SAV response (establishment, growth, and species assemblages) to drivers (i.e., model inputs) differs from emergent vegetation in both magnitude and time of response (DeMarco et al., 2021; Kinney et al., 2014; Cho & Biber, 2016) and as such required distinctive inputs from the vegetation modeling component. To meet the needs of the large-scale Coastal Master Plan modeling effort, the SAV model was developed with the specific goal to create inputs (percent cover) needed to drive the habitat suitability model components.

2.0 METHODS

2.1 STUDY AREA

The study area for this portion of the effort comprised a coastal zone seen below in Figure 1
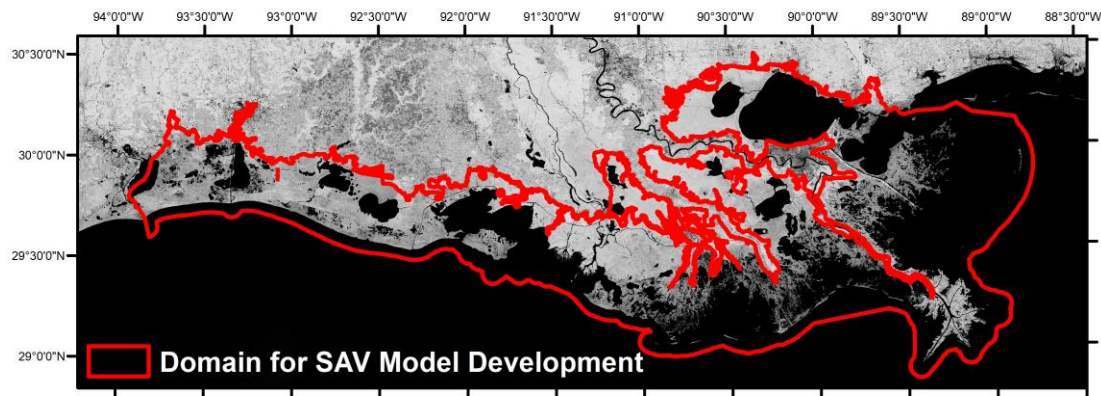
Figure 1. Map of Domain for SAV Model Development.

2.2 SPATIAL DATA

The occurrence and coverage of SAV is highly variable across large estuarine landscapes (DeMarco et al., 2021). The parameters known to influence the likelihood of occurrence of SAV including exposure, turbidity, depth, and salinity (among others) are spatially distinctive across and between regions, basins, and estuaries. As such, the model developed to forecast SAV must be informed by locally meaningful spatial data. This section will detail the creation of spatial data layers pertaining to the occurrence of SAV, as well as parameters known or suspected to influence SAV.

SAV PRESENCE/ABSENCE

The development of a model of a spatial likelihood of occurrence of SAV required large amounts of data describing areas in which SAV has likely occurred in the past. While in previous efforts (DeMarco et al., 2018) field data was used to estimate likelihood of occurrence, new remote sensing methods that provide extensive data points were used here. We developed a spatial data layer for current SAV conditions using a frequency of detection across the coast based on remotely sensed imagery (described below) and validated that layer and calibrated the model using field data from DeMarco et al. (2018).

The frequency of detection of SAV data layer was created from data sets available in Couvillion (2021). The methods involved in the detection of SAV are described further in the metadata of those data sets, but a brief summary is included below:

Remotely sensed detection of SAV is complicated by the fact that most wavelengths of light are rapidly attenuated by water. Detection of SAV can be further complicated by turbidity, including total suspended solids (TSS), water movement, and presence of floating aquatic vegetation (FAV). For these reasons, the detection of SAV in remotely sensed imagery on any given date is typically unreliable, except in particularly clear water conditions.

The detection of SAV over longer time periods however can be aided by the use of measures of variability in remotely-sensed signals or indices related to the presence of water and the presence of vegetation. We have observed measures of variability in the modified Normalized Difference Water Index (mNDWI), and the Normalized Difference Vegetation Index (NDVI) to be informative regarding the presence or absence of aquatic vegetation. An example of the standard deviation of all observations of the NDVI and mNDWI during a given year is shown in Figure 2. Areas with annual standard deviations exceeding threshold values of 0.24 and 0.22 respectively for the NDVI and mNDWI are often indicative of aquatic vegetation and these values were used to create masks of areas of possible aquatic vegetation.
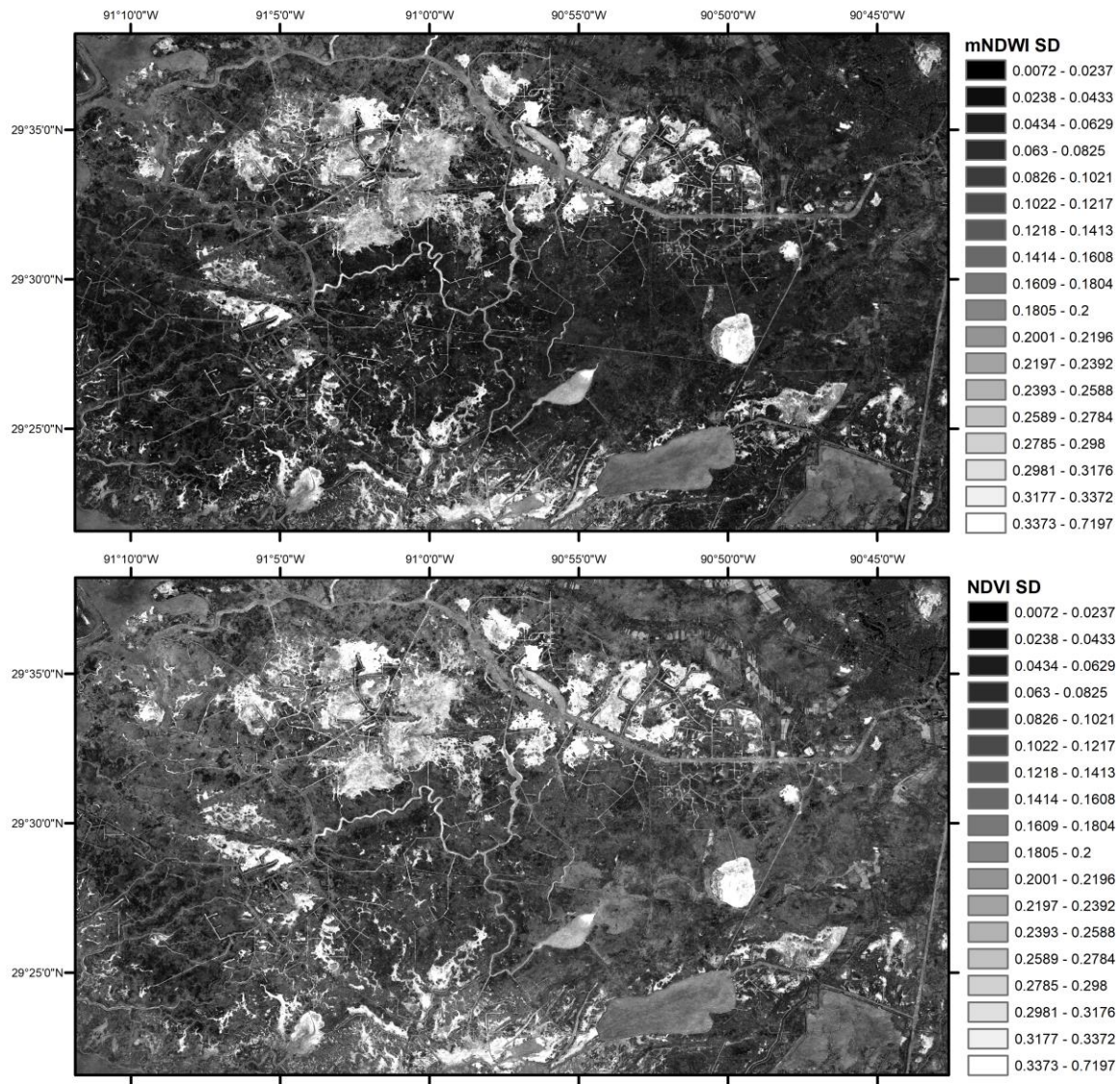
Figure 2. Standard Deviations of the NDVI and mNDWI during 2018 from Sentinel-2 Imagery. The number of observations varies in each pixel. Landsat has a revisit period of 16 days, thus leading to approximately 23 observations per year.   Some areas of the coast are covered in overlap of satellite images, thus increasing those areas to 46 observations per year. However, cloud cover and other sources of contamination necessitate the exclusion of many of those observations. The standard deviations displayed in Figure 2 draw from a mean of 18 observations per year (min:5, max:40).

While the aforementioned data sets are informative with regard to the presence of FAV and SAV

isolating those distinct types of vegetation requires further analysis. As such, these data sets were used in conjunction with spectral values, known as "endmembers" which are indicative of these categories, to further classify FAV and SAV. A process known as Multiple Endmember Spectral Mixture Analysis (MESMA) was used to estimate the fraction of each pixel comprised of wetland, FAV, SAV, and water (Adams et al., 1993; Roberts et al.,1993; Settle and Drake, 1993). Those fractional estimates are found in the individual bands and the data sets from Couvillion (2021).

As the observation period for this effort was selected as 2015 through 2018, the Couvillion (2021) data set was subset temporally to include only years during that time. These data sets were compiled and a frequency of detection of SAV from 2015 to 2018 was calculated (Figure 3). The data can be difficult to see at the coastwide scale displayed in Figure 3 and as such, gridded maps of the frequency of detection data set are available in Appendix 1.

Frequency of SAV Detection (2015-2018)

- 1%-33% of observations
- 34%-66% of observations
- 67%-100% of observations
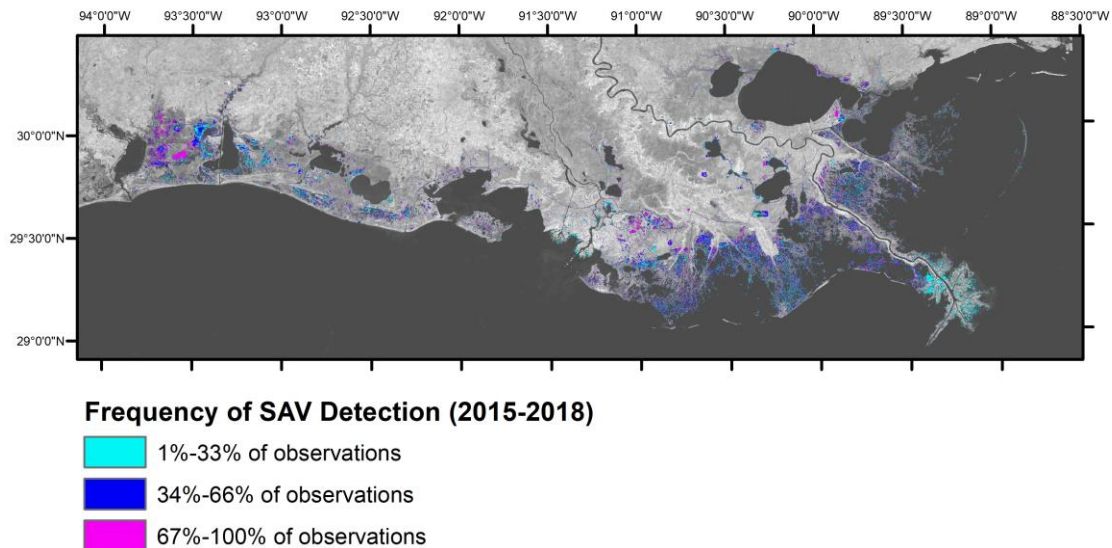
Figure 3. Frequency of SAV Detection (2015-2018).

As detection of SAV during any year within the 2015 to 2018 observation period is likely indicative of conditions suitable for the presence of SAV, detection (as indicated by frequency of detection exceeding 10% of observations) in any year was recoded to a presence category (Figure 4). The number of observations varies in each pixel, but greater than 97.8% of pixels have observations exceeding 12 observations per year with an overall pixel average of 23 observations per year. Some areas of the coast are covered in overlap of satellite images, thus increasing those areas to 46 observations per year. However, cloud cover and other sources of contamination necessitate the exclusion of many of those observations. The standard deviations displayed in Figure 2 draw from a mean of 18 observations per year (min:5, max:40). Because the frequency of SAV detection data layer is more vulnerable to errors of omission than those of commission, defining the presence category as detection in any year, rather than all years, or a majority of years, mitigates the impact of these errors

of omission. Water areas in which there were zero detections of SAV during the four observation years was recoded to an absence category.
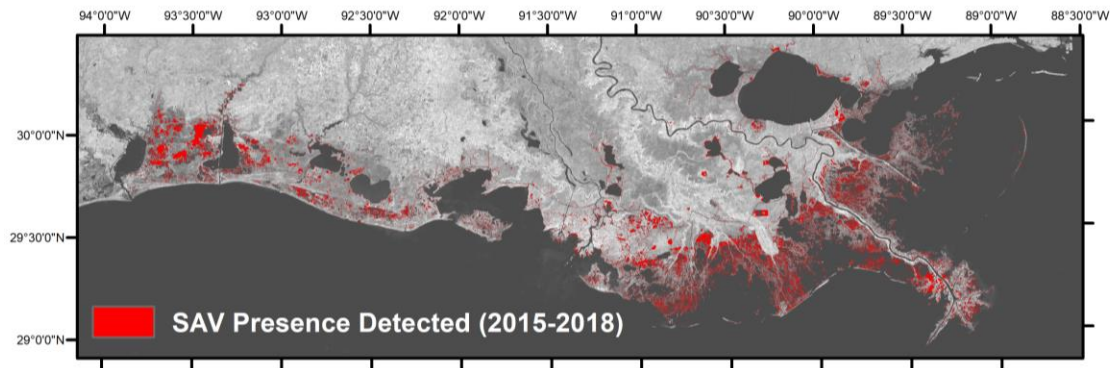
Figure 4. SAV Presence Detected (2015-2018).

SEASONAL TOTAL SUSPENDED SOLIDS (TSS)

Total suspended solids (TSS) concentrations influence the likelihood of occurrence for SAV by regulating light availability through the water column. While in general, increases in TSS that lead to decreases in light availability will decrease the likelihood of SAV, this is not the case for all species of SAV, particularly in dynamic estuaries. TSS can vary dramatically in coastal environments, and many species found in the Louisiana coastal zone are adapted to these fluctuations in water clarity (DeMarco et al., 2021; Holm Jr & Sasser, 2001; Kolker et al., 2018). Light availability is the key driver of SAV presence/occurrence, and result of the interaction between both TSS and depth. At shallow depths, high TSS may not have as great an impact on occurrence, while at high depths, TSS will have a stronger effect through regulating light penetration.

We observed significant seasonal variation in turbidity across coastal Louisiana through spectral reflectance (DeMarco et al., 2018), and observed related seasonal impact on growth, establishment and occurrence of SAV. While some monitoring programs do collect TSS, the spatial distribution and temporal frequency of such data collections is insufficient to interpolate seasonal spatial data sets. Given these limitations, we replicated methods in the DeMarco et al. (2018) (Summer=May 15 – September 14 (daily mean water temperature >25°C), Fall=September 15 – November 14 (daily mean water temperature range=24°C – 16°C), Winter=November 15 – February 14 (daily mean water temperature < 15°C), and Spring=February 15 –May 14 (daily mean water temperature range=16°C – 24°C)) in an effort to determine TSS across the coast. This method assumes correlations between the red wavelengths of light and TSS. Previous investigations have used similar hyperspectral imagery methods to estimate TSS (Jensen et al., 2022). While this effort produced a spatially variable estimate of TSS that was able to be applied to meet master plan needs, the limited time periods and portion of coastal Louisiana area evaluated did not provide complete spatial or

temporal coverage. To fill these gaps, we combined the spatial data from Jensen et al. (2022) with modeled TSS estimates from Delft-3D Mid-Barataria Sediment Diversion modeling efforts. We intersected those TSS values with moderate-resolution (30-meter) Landsat-8 Surface Reflectance imagery from similar time periods to develop a relationship between TSS (mg/L) and reflectance in Band 4 of the Landsat imagery. The resulting equation is shown below in Equation 1.

$$TSS(mg/L) \ = \ 2.24796943e0.00419007 \ (Landsat - 8 \ B4)$$
$$R^2 \ = \ 0.619$$

Equation 1. Formula for estimating TSS from Landsat-8 B4.

The resulting formula estimates of TSS for every cloud-free date of Landsat-8 imagery from 2015 through 2018. The resulting spatial data sets were then averaged seasonally (Figure 5).
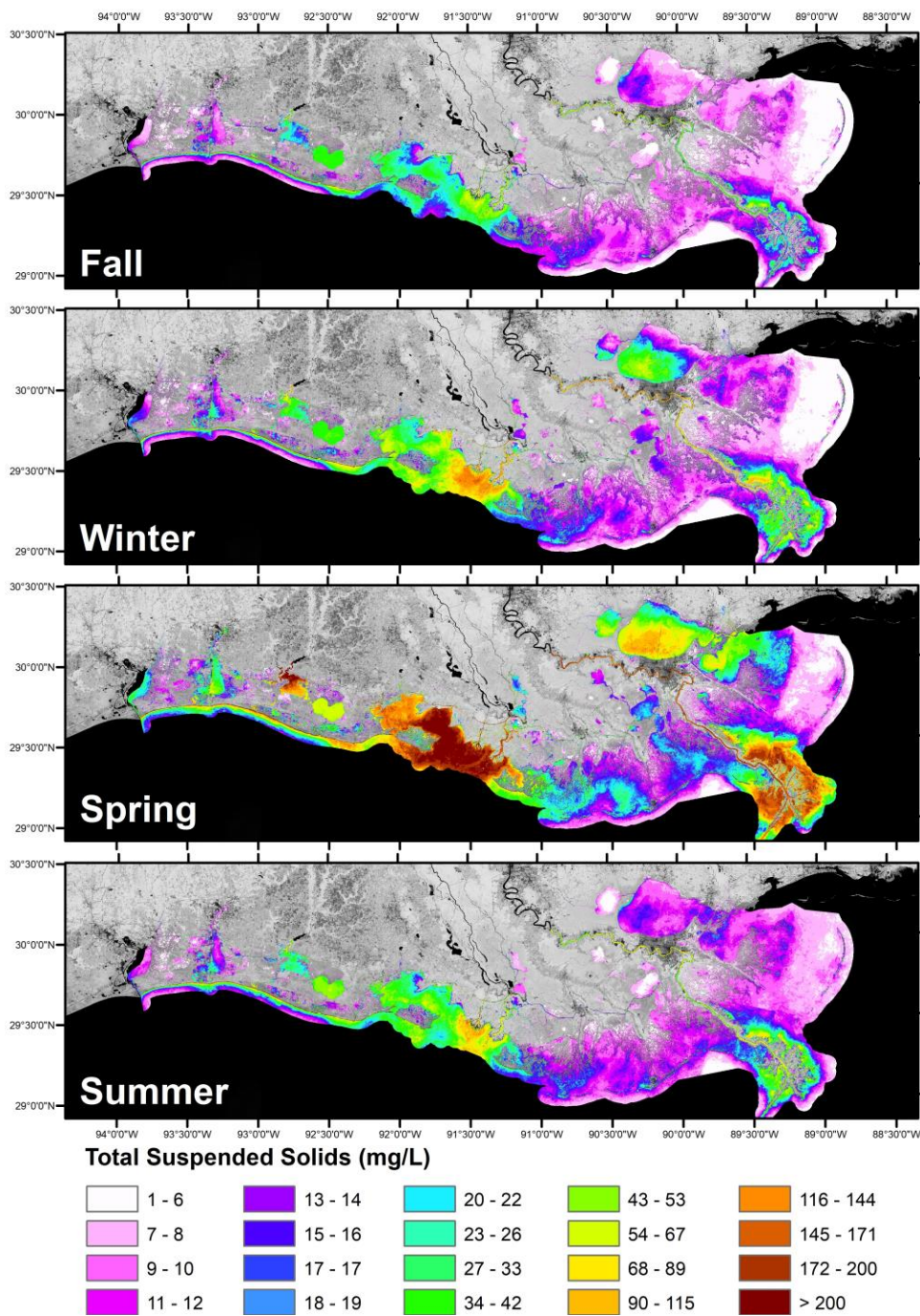
Figure 5. Season Total Suspended Solids (mg/L) Estimated via Landsat 8 Imagery.

SALINITY – SEASONAL AVERAGE

The seasonal salinity data leveraged data sets created as part of the work described in Swam et al. (2022). These daily salinity data were interpolated from various sources including continuous data recorders from the Coastwide Reference Monitoring System (CRMS; CPRA, 2021) the United States Geological Survey (USGS, 2021) (Figure 6). Offshore data were obtained from the Hybrid Coordinate Ocean Model for salinity (GODAE, 2021) (Figure 6). For each source, daily salinity were obtained from January 1, 2015 through December 31, 2018 (See Swam et al., 2022 for more details).
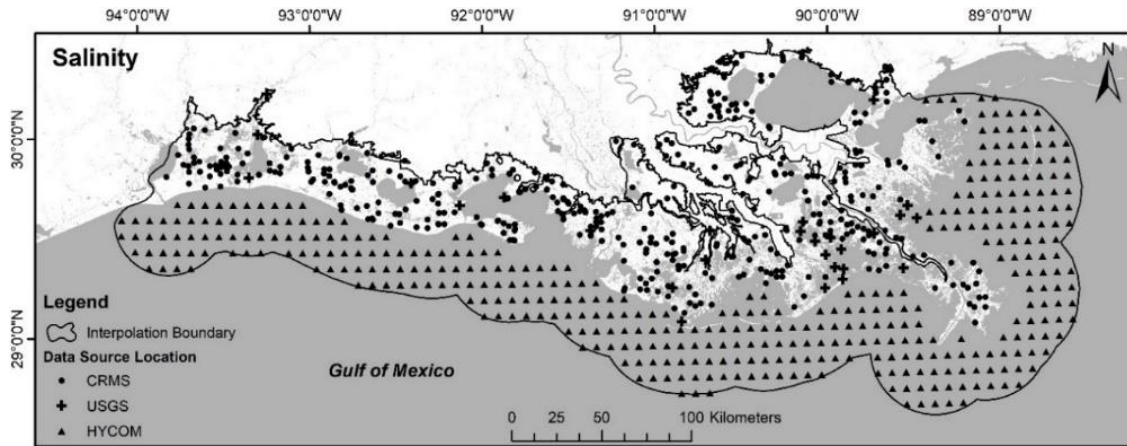
Figure 6. Salinity Data Locations of 457 CRMS Data Recorders (CPRA, 2021), 27 USGS Data Recorders (USGS, 2021), and 392 Data Points from HYCOM (GODAE, 2021) for 2015-2018. (Adapted from Swam et al., 2022.)

Daily salinity data was interpolated using a spline with barriers. This technique estimates a surface in which the value passes through the input points exactly, while minimizing curvature of the surface between points. Barriers were enforced to prevent interpolation across features such as levees, impoundments, and basins (DeMarco et al., 2018). The resulting interpolated daily salinity surfaces were averaged seasonally to create means on a per pixel basis (Figure 7).
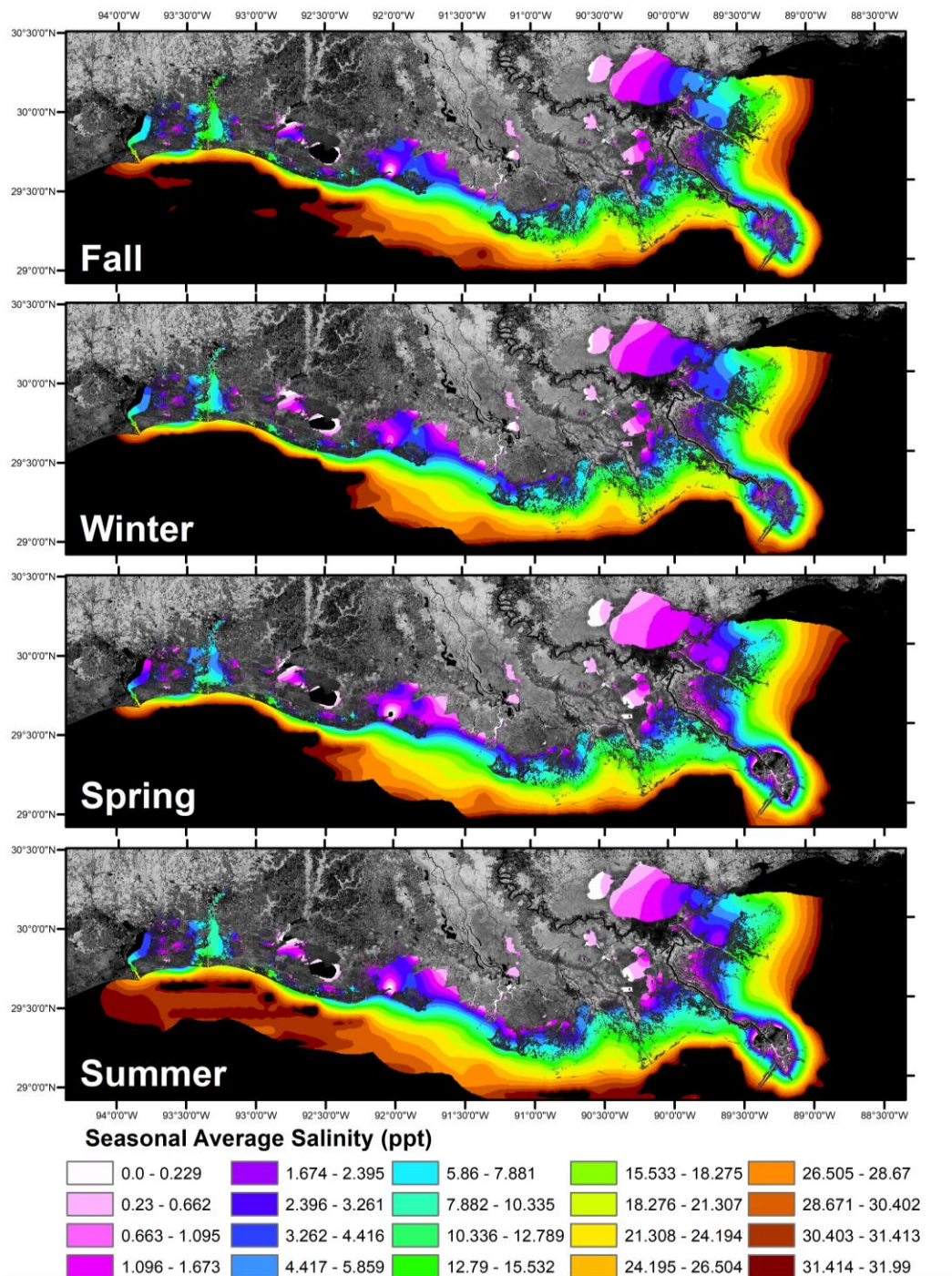
Figure 7. Seasonal Average Salinity (ppt), interpolated from daily data including CRMS, USGS, and modeled HYCOM data offshore. Salinities above 32 ppt are not depicted in this visualization.

DISTANCE TO LAND

Exposure to wave energy and other physical processes are other forces known to influence the likelihood of occurrence of SAV; often via influence on establishment (e.g., current velocities). All other parameters being equal, greater exposure to wave energy lowers the likelihood of occurrence of SAV in estuarine environments/coastal Louisiana. A complete calculation of exposure requires a calculation of wave energy which is dependent upon fetch, wind speed, direction and duration, and bathymetry. Moreover, these calculations are needed at fine time intervals (i.e. minutes), and are consequently computationally intensive.

While exposure would have been the more appropriate parameter, early discussions regarding the feasibility of calculating exposure at the spatial and temporal scales of the model indicated such computationally intensive calculations would not be feasible. We therefore investigated distance to land as a proxy related to exposure. While distance to land is not directly a measure of exposure, it captures a good part of the variation caused by exposure and has been shown to relate to SAV presence (DeMarco et al., 2018), and in many cases, areas with smaller values of distance to land are often less exposed. Distance to land is easily calculated and computationally efficient, and as such, this proxy was used for 2023 Coastal Master Plan SAV modeling efforts.

Distance to land for the baseline observation period was calculated using a mean 2015 to 2018 landscape composition. A simple Euclidean distance calculation was performed to calculate the straight-line distance from each water pixel to the nearest land pixel. An example from the resulting spatial data set is shown below in Figure 8.
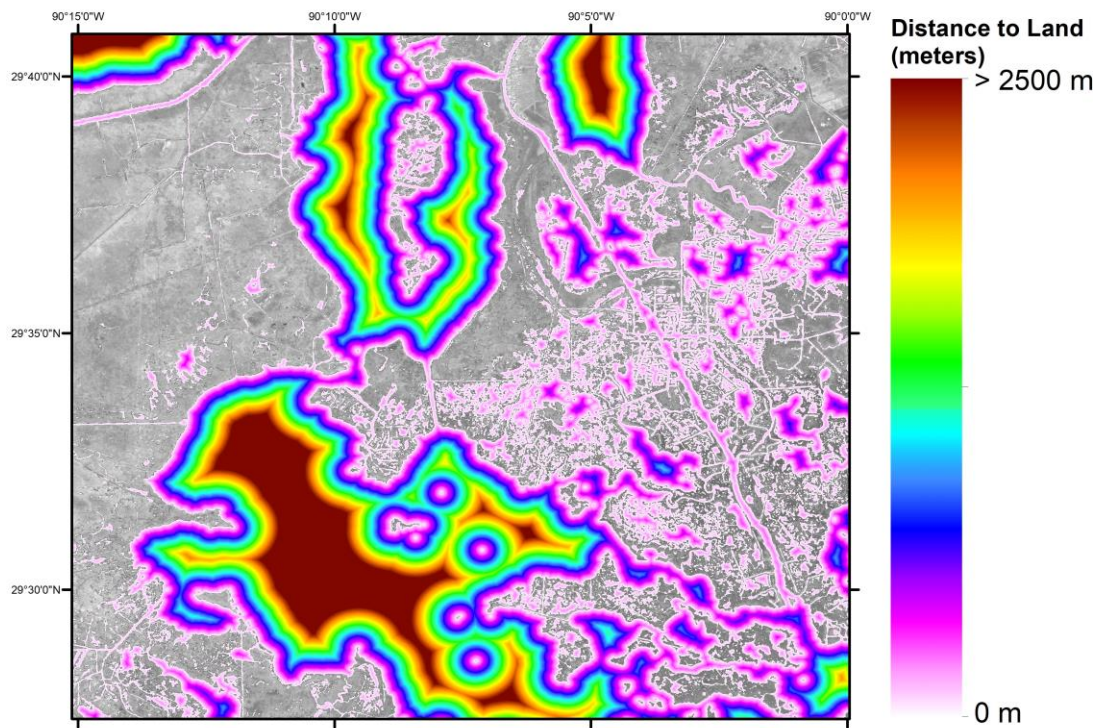
Figure 8. An Example from the Distance to Land Data Layer (2015-2018 median conditions).

BASIN

Coastal Louisiana contains 9 broad hydrologic basins originally delineated by CWPPRA (Figure 9). Many processes and parameters of interest that influence SAV vary in these basins but are complicated to quantify and can result in confounding variables for statistical analyses. and the historical influence of basin characteristics and conditions. As such, it was suspected that basin may be a valuable categorical value representing a proxy for these complex conditions which the SAV model might use in a predictive capacity. We therefore included a value for basin when intersecting the points.
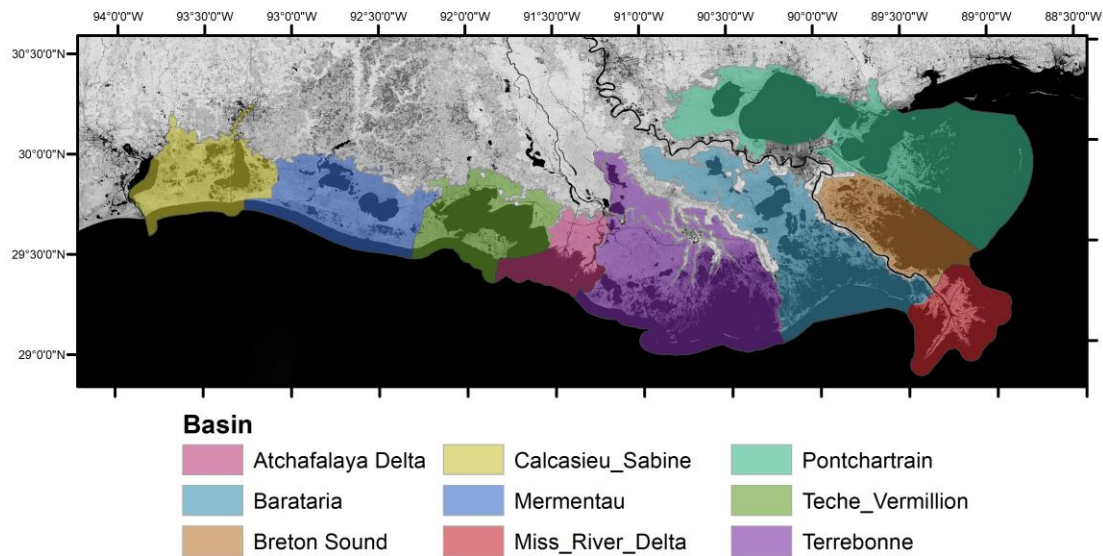
Figure 9. Coastal Louisiana Basins.

SAMPLE

A random, stratified SAV presence/absence sample was taken from the data set described in the SAV Presence/Absence section above and intersected with the spatial layers described in the Seasonal Total Suspended Solids (TSS) section through the Basin section. The sample originally included 500,000 points, shown below in Figure 10.

SAV Detection (2015-2018)
- SAV Present
- SAV Absent
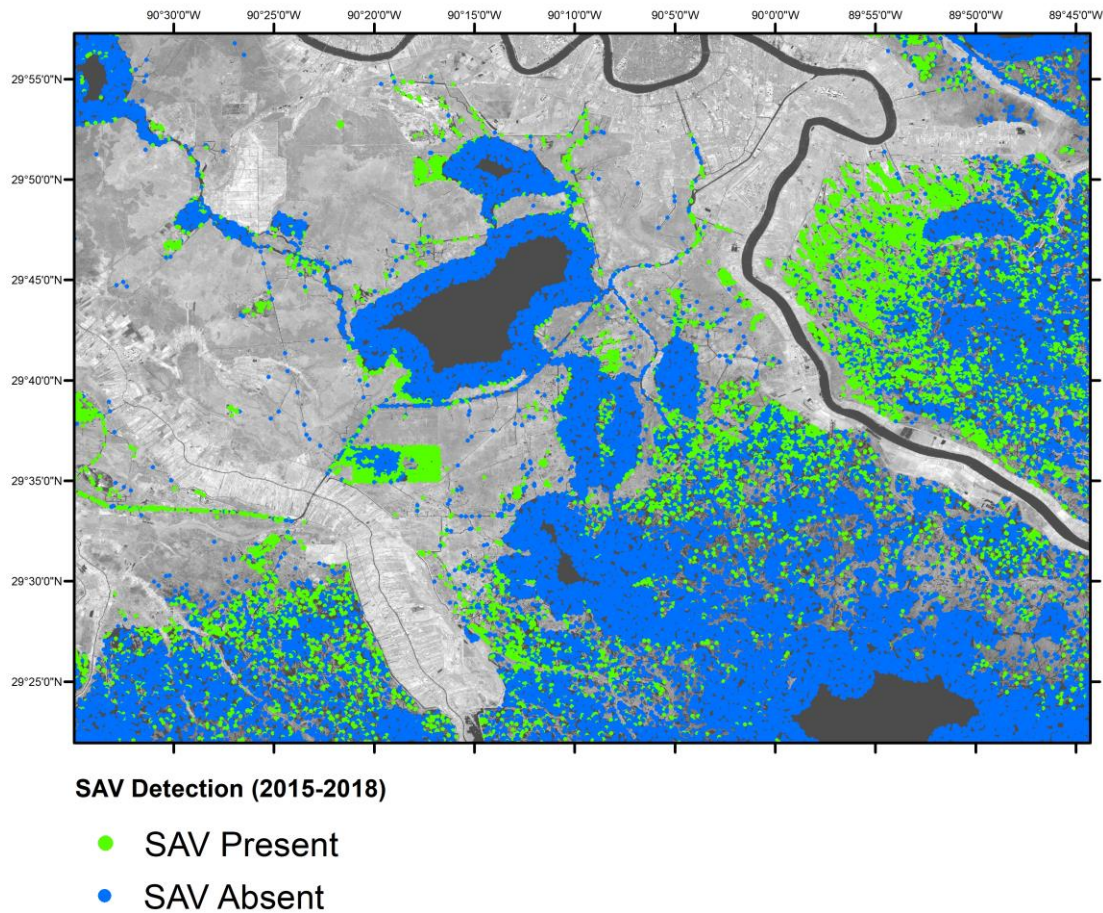
Figure 10. An Example of the Randomly Selected SAV Presence/Absence Points.

2.3 MODEL DEVELOPMENT

Here, we used the remotely sensed data (described above) to develop and model to predict the presence of SAV at the 30 m x 30 m spatial scale.

MODELING FRAMEWORK

We chose to use a Naïve Bayesian framework for this task. Naïve Bayesian models are generative classifiers (Ng & Jordan, 2001). That is, for a set of predictors, $X = \{X_1, X_2, ..., X_n\}$ and categorical response Y, calibration data are used to learn the distributions P(X|Y) and P(Y). These are then used to calculate $P(Y|X)$ using Bayes Rule,

$$P(Y|X) = \frac{\prod P(X|Y)P(Y)}{P(X)},$$

where $P(Y)$ is the prior probability y and $P(X)$, in the case of a binomial response, is the constant

$P(X) = \prod P(X|y = 1)P(y = 1) + \prod P(X|y = 0)P(y = 0)$. Naïve Bayesian classifiers make the strong simplifying assumption that all the predictors are independent due to the response, i.e., $P(X_1|X_{2,}, y = 1) = (X_1|y = 1)$. Despite the strong nature of this assumption, in practice, Naïve Bayesian classifiers often show robust performance and are often more efficient at smaller training samples than discriminant classifiers, such as logistic regression (Ng & Jordan, 2001). To classify a sample, X, the naïve Bayes classifier $h: X \mapsto Y$ predicts $h(x) = 1$ if and only if

$$log \frac{\prod P(X|y = 1)P(y = 1)}{\prod P(X|y = 0)P(y = 0)} > 0.$$

MODEL SELECTION

The data were split into a calibration sample of 250,000 cases and a test sample consisting of the remaining cases except those with any missing data. The final size of the test sample was 25,248 rows. The initial set of environmental predictors included 12 measures developed from the spatial data (described above): 4 seasonal salinity measures, 4 seasonal measures of TSS, 3 measures of fetch (min, max, standard deviation), and distance to land. We used multiple criteria to narrow this set to those to be included in the model. First, since we hoped to only include predictors of SAV thought to be important drivers, we removed those predictors thought to be responses of SAV or with a potentially ambiguous relationship to SAV and/or were significantly correlated with one another. For example, SAV in our study area generally germinates in the spring season (based on water temperature/seasonal data), and once stands are established the plants are not as sensitive to changes in salinity and turbidity/TSS, so these variables ecologically would be less influential. This criterion resulted in the removal of Summer TSS, Fall Salinity and Summer Salinity, as ecologically these values were less critical in driving occurrence and further were highly correlated with other variables/seasons. Next, we wanted to minimize the computational load of the model while in production. This required that we consider the computational complexity of deriving each predictor. Of the remaining variables, in the context of the modeling environment of the master plan, those variables representing different aspects of fetch are much more computational complex than the others; thus, they were removed from the set.

We used a quantitative method to choose among the remaining variables. The strategy was as follows, (1) fit each variable as a function of Y, (2) use the residuals of those fits to perform a cluster analysis, such that each variable has higher residual correlation with other variables within its cluster than with those in other clusters, (3) use R_i^2 to select a variable from each cluster. This process attempts to maximize the performance of the naïve Bayes classifier by selecting variables with high correlation with SAV presence and low residual correlation with the other variables in the selection set.

Before estimation, each remaining variable, X, was log-transformed to X'. Then for each X', the quantity $\hat{P}(X'|Y)$ was estimated using simple linear regression. To perform clustering, the residuals of these models, $\hat{\varepsilon} = X' - \widehat{X'}$, were estimated. The matrix $1 - |cor(\hat{\varepsilon})|$ was used as the distance matrix to perform hierarchical clustering with the hclust() function on the R platform (R Core Team, 2021). We chose the threshold 0.25 as the height at which the resulting tree should be cut to determine final

groups. This resulted in three groups: One containing the remaining seasonal salinity measurements (spring and winter), one containing the remaining seasonal TSS measurements (fall, spring, and winter), and one consisting of distance to land. Selecting the variable with the highest R_i^2 from each group resulted in a final set consisting of spring salinity, distance to land, and spring TSS. The fitted parameters for the fits of each of the selected variables are shown in Table 1. Ecologically, the significant influence of spring variables on SAV is reasonable, as many species are more sensitive to light availability, disturbance, and stress during the seedling/germination stage (Doyle & Smart, 2001; Hillmann et al., 2019; Jarvis & Moore, 2008; Strasizar et al., 2013).

MODEL BASIN PRIOR ESTIMATION

To capture additional geographical and historical factors in the classifier, we calculated a different value for the prior conditions, $P(Y)$, for each combination of hydrological basin and vegetation community type as defined by the FFIBS score for the vegetation community of the nearest the target pixel (Table 1). Essentially, the priors give an estimate of probability (by basin) before intervention/changes to conditions as determined by the environmental variables and inputs for the final model. These basin priors were calculated from the calibration data using logistic regression as the conditional probability of SAV.

Table 1. Parameters of $\hat{P}(X'|Y)$ for selected predictor variables

	SPRING SALINITY	DISTANCE FROM LAND	SPRING TSS
Intercept	1.106	5.825	3.423
Slope	-0.927	-1.945	-0.797
Residual SD	1.511	1.354	0.980

PREDICTOR IMPORTANCE ANALYSIS

To examine the effect of geographical information in the basin prior and each of the predictors on model performance, we generated predictions for each of the cases in the testing data for sub-models where one element, either the prior or one predictor, was removed (Table 2). As with the full model, we calculate the accumulate cases within basins to help determine how the importance of each parameter may vary along the coast.

Table 2. Effects of removal of basin priors

Hydrologic Basin	Intercept	Slope
Atchafalaya Delta	-1.780	-0.289
Barataria	-1.158	-0.067
Breton Sound	0.569	-0.178
Calcasieu-Sabine	1.371	-0.256
Mermentau	-1.165	-0.076
Mississippi River Delta	-0.727	-0.333
Pontchartrain	-1.327	-0.105
Teche-Vermilion	-1.391	-0.182
Terrebonne	0.522	-0.146

3.0 RESULTS

3.1 RESULTS SUBSECTION

We applied the naïve Bayesian classifier defined by the prior and set of fitted distributions of the environmental variables to the test data to quantify its performance. The resulting confusion table for one partition of the data is shown in Table 3 and visualized in Figure 11. The confusion table corresponds to a correct classification rate (ccr) of 0.898 and kappa statistic of 0.580. Kappa is a standardized statistic that compares the model's accuracy to an expected accuracy, where values closer to 1 indicate better fit. For example, if a classifier has a ccr of 0.75 and the expected performance of a random classifier is a ccr of 0.5, then the test classifier has a kappa statistic of 0.5, which means it accounts for 0.5 of the incorrect classification rate of a random classifier.

Table 3. Confusion matrix resulting from applying the Naïve Bayesian classifier to the 25,248 cases in the testing data set

	Observed	
Predicted	Absent	Present
Absent	20387	1334
Present	1297	2230

Figure 11. Distributions of the Predicted Probability of SAV Presence in the Test Data Set Conditional on its Actual Presence. The boxes show the interquartile range. The thick black lines show the medians, and the whiskers show the minimum and maximum of non-outliers in each group.

To examine the performance of the model geographically, we calculated both the ccr and kappa statistic for each of the hydrological basins (Table 4). For all basins, except Atchafalaya Delta, the Kappa statistic was near 0.5 or greater, indicating generally good performance across the coast, but with potential room for improvement in the Atchafalaya Delta Basin.

Table 4. Correct Classification Rate (CCR) and Kappa Statistic for the Naïve Bayesian Classifier tallied by hydrological basin

Hydrologic Basin	CCR	Kappa
Atchafalaya Delta	0.91	0.238
Barataria	0.895	0.465
Breton Sound	0.864	0.642
Calcasieu-Sabine	0.797	0.522
Mermentau	0.914	0.683
Mississippi River Delta	0.911	0.487
Pontchartrain	0.942	0.467
Teche-Vermilion	0.933	0.49
Terrebonne	0.896	0.62

PREDICTOR IMPORTANCE ANALYSIS

Removal of the geographic information, in the form of the prior, or any of the three predictors reduced both the correct classification rate and the kappa statistics (Figure 12). Removal of the prior had the biggest negative impact on the ccr, although in absolute terms the difference was quite small (Figure 12a). Removal of distance to land from the model had the largest impact on the kappa statistics, reducing it from kappa=0.552, for the full model, to kappa= 0.409 (Figure 12c). At the basin-scale, removal of predictors has little effect on the ccr, which is quite high under all conditions (Table 5), but removal of predictors has large and varying effects on the kappa statistic (Table 6). For example, for the Mississippi River Delta Basin, the removal of the geographic information in the prior, spring salinity, or distance from land causes large reductions in the kappa statistic reducing it from 0.487, to 0.196, 0.094, and 0.02, respectively. Removal of distance from land also had large effects of the performance of the model in the Atchafalaya Delta Basin, reducing kappa from 0.238 to 0.03, Pontchartrain (from 0.467 to 0.09), and Teche-Vermilion (from 0.49 to 0.03).
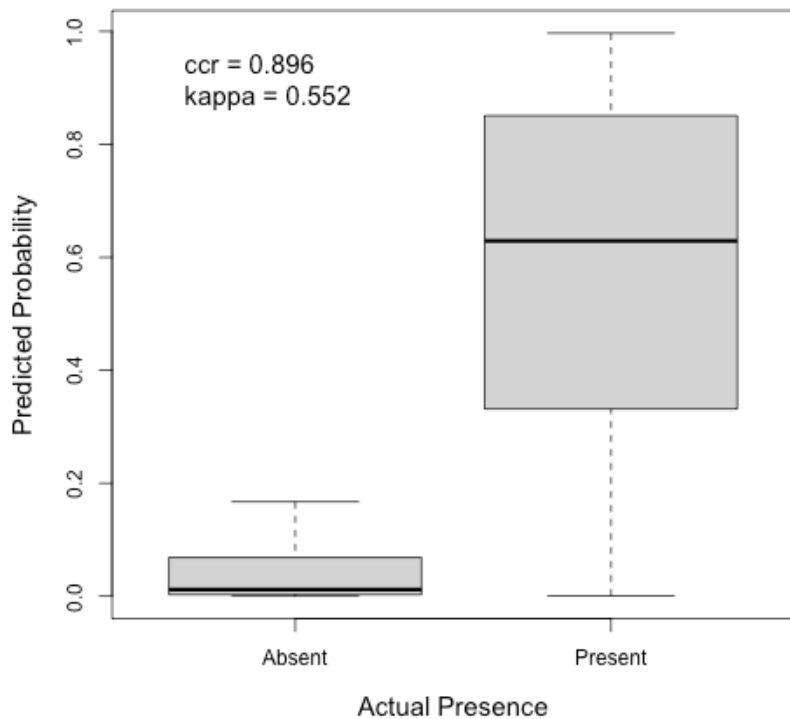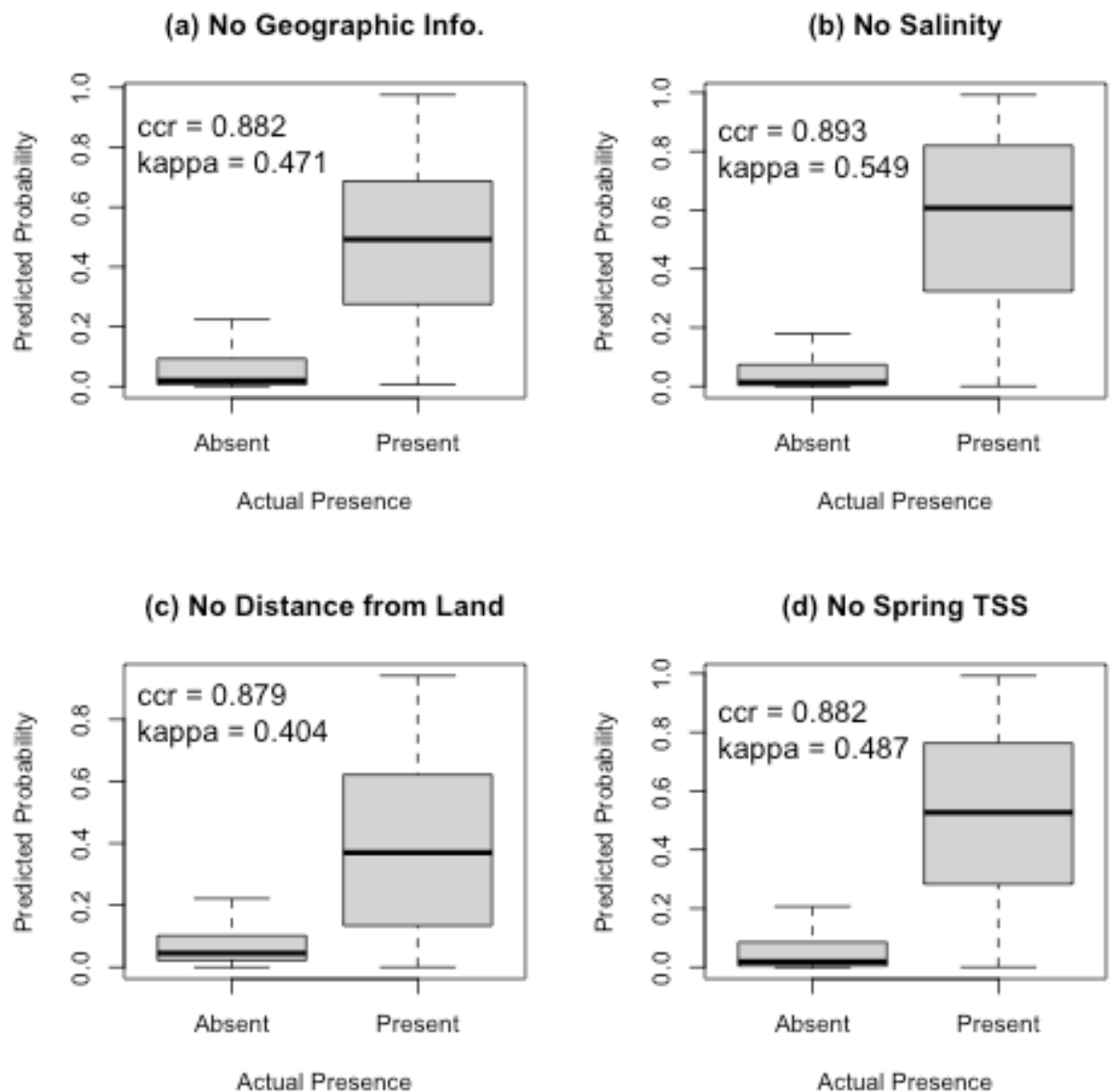
Figure 12. Distributions of the Predicted Probability of SAV Presence in the Test Data Set Conditional on its Actual Presence Resulting from the Removal of Individual Predictors. The boxes show the interquartile range. The thick black lines show the medians, and the whiskers show the minimum and maximum of non-outliers in each group.

Table 5. The basin-scale correct classification rate resulting of removing predictors

HYDROLOGIC BASIN	NO GEOGRAPHIC INFO.	NO SALINITY	NO DIST. FROM LAND	NO SPRING TSS
Atchafalaya Delta	0.935	0.929	0.92	0.92
Barataria	0.885	0.888	0.87	0.893
Breton Sound	0.821	0.841	0.86	0.828
Calcasieu-Sabine	0.741	0.791	0.81	0.788
Mermentau	0.914	0.917	0.88	0.88
Mississippi River Delta	0.885	0.883	0.88	0.883
Pontchartrain	0.926	0.935	0.94	0.933
Teche-Vermilion	0.926	0.925	0.93	0.933
Terrebonne	0.875	0.892	0.86	0.878

Table 6. The basin-scale correct classification rate resulting of removing predictors

HYDROLOGIC BASIN	NO GEOGRPAHIC INFO.	NO SALINITY	NO DIST. FROM LAND	NO SPRING TSS
Atchafalaya Delta	0.374	0.2	0.03	0.474
Barataria	0.452	0.423	0.18	0.346
Breton Sound	0.46	0.575	0.59	0.517
Calcasieu-Sabine	0.309	0.542	0.54	0.508
Mermentau	0.625	0.65	0.29	0.509
Mississippi River Delta	0.196	0.094	0.02	0.458
Pontchartrain	0.484	0.411	0.09	0.311
Teche-Vermilion	0.409	0.309	0.03	0.445
Terrebonne	0.5	0.618	0.44	0.549

4.0 DISCUSSION

Developing a model to represent assemblages of SAV across a large wetland landscape spanning a dynamic ecosystem with distinct environmental and ecological gradients (e.g., coastal Louisiana) is a challenging task. Individual species and assemblages of species of SAV respond to changes in environmental conditions based on their unique species physiology – developing a model to represent all possible species across a large coastal landscape required input from experts in ecology and spatial and statistical analyses as well as knowledge of data sets collected in-situ from field experiments in combination with remotely sensed imagery. This iteration of the SAV model achieved the goal of being as simple as possible while maintaining an acceptable level of accuracy across a large and dynamic landscape. Applications of these results should be evaluated in that context.

This model demonstrated high levels of accuracy across the study area, differing significantly from a random classifier, as indicated by the high ccr and kappa statistic. Additional measures (Table 7) explain that this model performed especially well at predicting absence (true negative = 0.940), and, while still biologically meaningful, performed less well at predicting presence (true positive/sensitivity rate = 0.626). Lowered performance at predicting presence can likely be attributed to the relatively low instances of SAV presence across the study area (i.e., all of coastal Louisiana) as indicated by a low prevalence rate (0.141). The prevalence rate performance measure describes how often presence was actually observed, and here, indicates that most of the training data used to design the model were absence values. This suggests that the spatial scale of the model limits the ability for increased accuracy at predicting presence. For increased accuracy describing presence, smaller scale models, either in unique basins or aquatic zones (discussed later) may be helpful.

We further evaluated model performance by examining the spatial estimates of likelihood of occurrence and change in likelihood of occurrence as determined by the input variables at 3 timesteps – initial (Y02, Year 26, and the final timestep (Y52). The model performed as expected in response to the driving variables with likelihood of occurrence decreasing in response to increases in spring salinity, spring TSS, and distance to land. In other words, changes in probability of SAV occurrence over time (Figure 13) are reflective of predicted changes in these conditions, e.g., model inputs. Notable areas of interest include Sabine Lake in western Louisiana, and areas of significant freshwater outflow. In Sabine Lake (Figure 14), likelihood of SAV is predicted to increase markedly from initial conditions (Y02) to final model year (Y52). Currently, Sabine Lake supports virtually no SAV (DeMarco et al., 2018 and 2021) presumably due to a combination of salinity and turbidity factors, so these results were unexpected. Spatial review of the model inputs show that spring salinity is predicted to decrease significantly around Sabine Lake, leading to the increase in likelihood of occurrence, the model performing as expected. Overall, there was low probability of occurrence for initial conditions (Figure 15a) around freshwater outflow areas (e.g., the Mississippi River, Wax Lake, Atchafalaya deltas, and the Davis Pond Freshwater Diversion), and a decrease in future probability estimates of occurrence. Observed data indicate that this is currently not the case, and that SAV is

generally present, sometimes in abundance, where depth is not preventative. Analysis of the model input as spatial layers show these areas were experiencing high TSS loads both initially (Figure 14b) and in future, which is realistic, but this resulted in a dramatic reduction in modeled SAV occurrence, which is not always the case. This model appears to underestimate occurrence at the outflow of diversions and freshwater sources, a problem that is likely pervasive in modeling SAV across outflow areas in dynamic estuaries. Model improvements in future efforts may include more localized models or models tailored to diversion and/or more dynamic environments.

Another potential benefit of examining more localized models can be demonstrated by the relatively large impact of removing the basin prior on the kappa statistic. When we removed the basin priors the kappa statistic decreased (Figure 12a), indicating that the complex basin conditions influence the presence of SAV across the coast. Basin priors represent both historic or long-term conditions and overall regimes in each geographic region. While SAV does respond quickly to changes in geomorphology and water quality, these longer term conditions and regimes can essentially serve as a background landscape for the establishment of SAV, and influence the likelihood of occurrence. Each basin appears to support unique combinations of SAV that are responding to similarly unique conditions and the basin priors function as proxies for the suite of environmental and biological factors that influence species assemblages and SAV establishment. Moreover, these basins are reflective of current conditions and past conditions, capturing the legacy of SAV establishment and communities that develop from historic patterns (which are notoriously difficult to measure/estimate). Depending on the level of accuracy and spatial scale needed, SAV occurrence models could be developed on a basin scale that reflect the unique conditions throughout. Potential improvements for specific basins may be possible with the inclusion of additional predictor variables. A list of which candidate variables to test should be selected by system experts.

Data and modeling from other efforts indicate that physical exposure, specifically wave power and fetch, has a significant impact on SAV occurrence in coastal areas (DeMarco et al., 2018; Fonseca & Bell, 1998; Gurbisz et al., 2016; Pulich & White, 1991; Robbins & Bell, 2000; Santos et al., 2011). For this effort, fetch was not logistically feasible as it was too computationally intensive to obtain, due to both time steps and spatial scale. For these master plan needs, the distance to land function proved to be sufficient at given the scale and end purposes. If more accuracy and greater degree of spatial resolution was desired, the inclusion and/or improvement of fetch calculation should be incorporated.

In general and overall, more precise results would be possible in a scaled down model used for local applications using field derived data in combination with remotely sensed data. This model version provided a coarse resolution SAV data representing a large coastal landscape. Identifying aquatic zones similar to the emergent marsh classifications described by FFIBS, either by basins or at other spatial scales, and identifying a representative SAV species (DeMarco et al., 2021) could provide more accurate modeling results as well as quickly describe aquatic conditions including long-term salinity and as well as salinity variability, water depth, and exposure.

Understanding how changes in key environmental drivers influence SAV occurrence, distribution, and

coverage are critical to our ability to predict possible future alterations to ecological structure (i.e., trophic webs) and develop restoration and protection plans accordingly. While outputs from this SAV modeling effort are largely generated to provide habitat information, these habitats are increasingly recognized for benefits beyond those that they provide to fish and wildlife species. SAV community assemblages represent unique aquatic habitats which differ from more commonly discussed emergent marsh zones that are classified by long-term salinity and hydrology.

Table 7. Additional performance measures from confusion matrix

Measure	Value
Accuracy/CCR	0.896
Misclassification	0.104
True positive/Sensitivity	0.626
False positive/Specificity	0.060
True negative	0.940
Precision	0.632
Prevalence	0.141

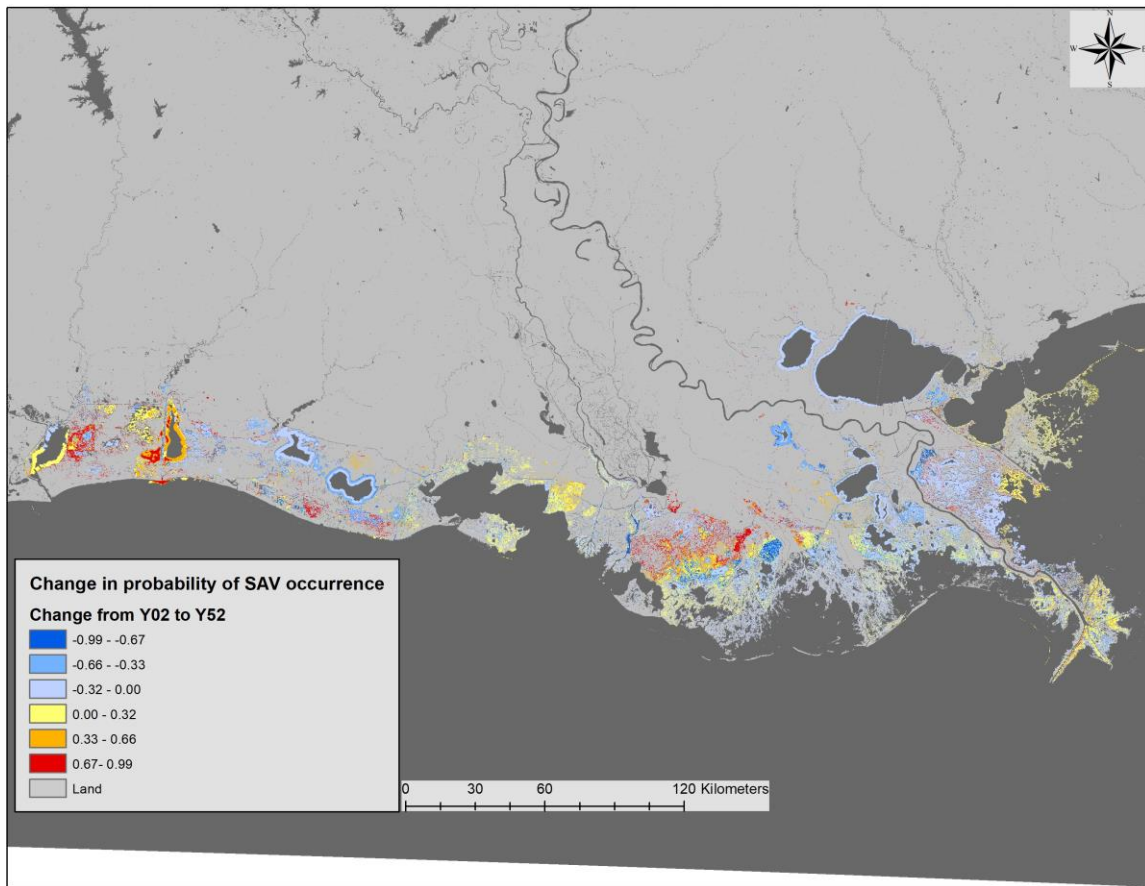Figure 13. Change in Probability of Occurrence of SAV from Initial Conditions (Y02) to Final Time step (Y52).
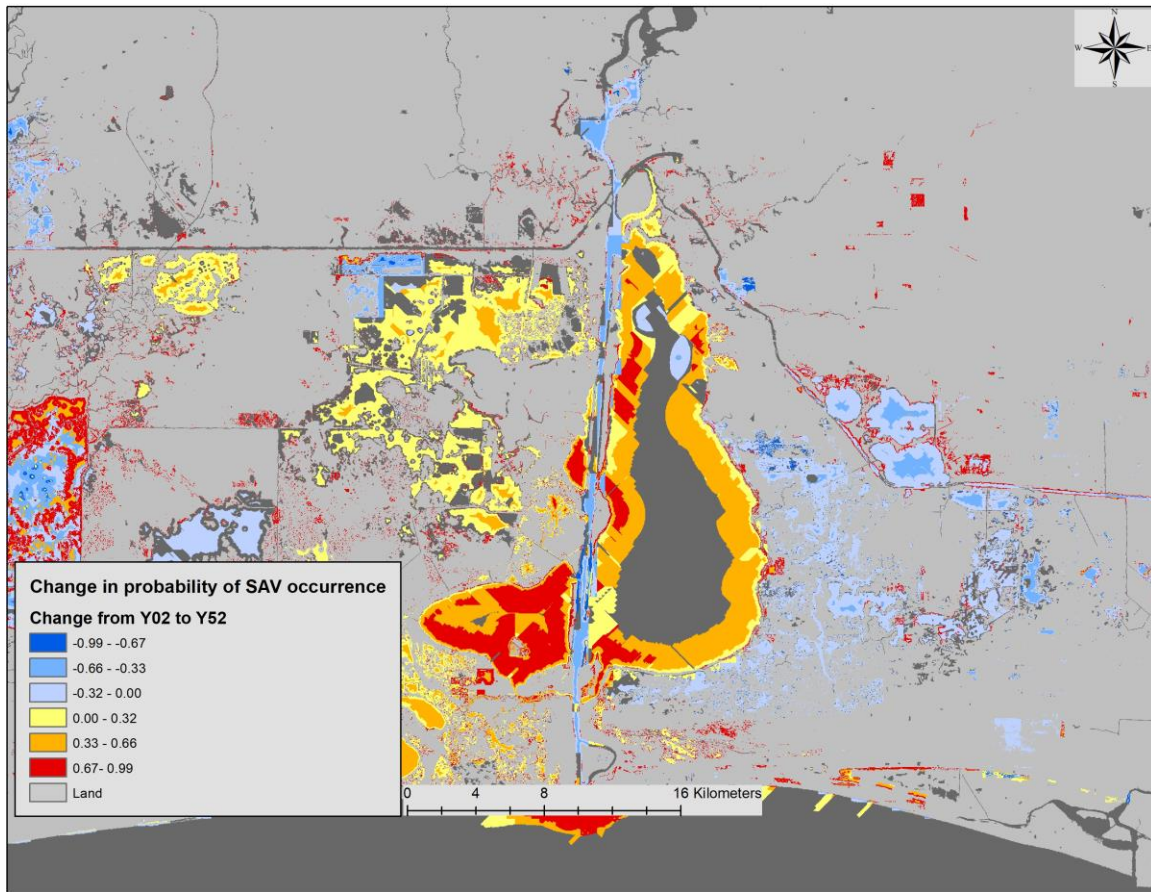
Figure 14. Change in Probability of Occurrence of SAV from Initial Conditions (Y02) to Final Time Step (Y52) in Sabine Lake, LA.
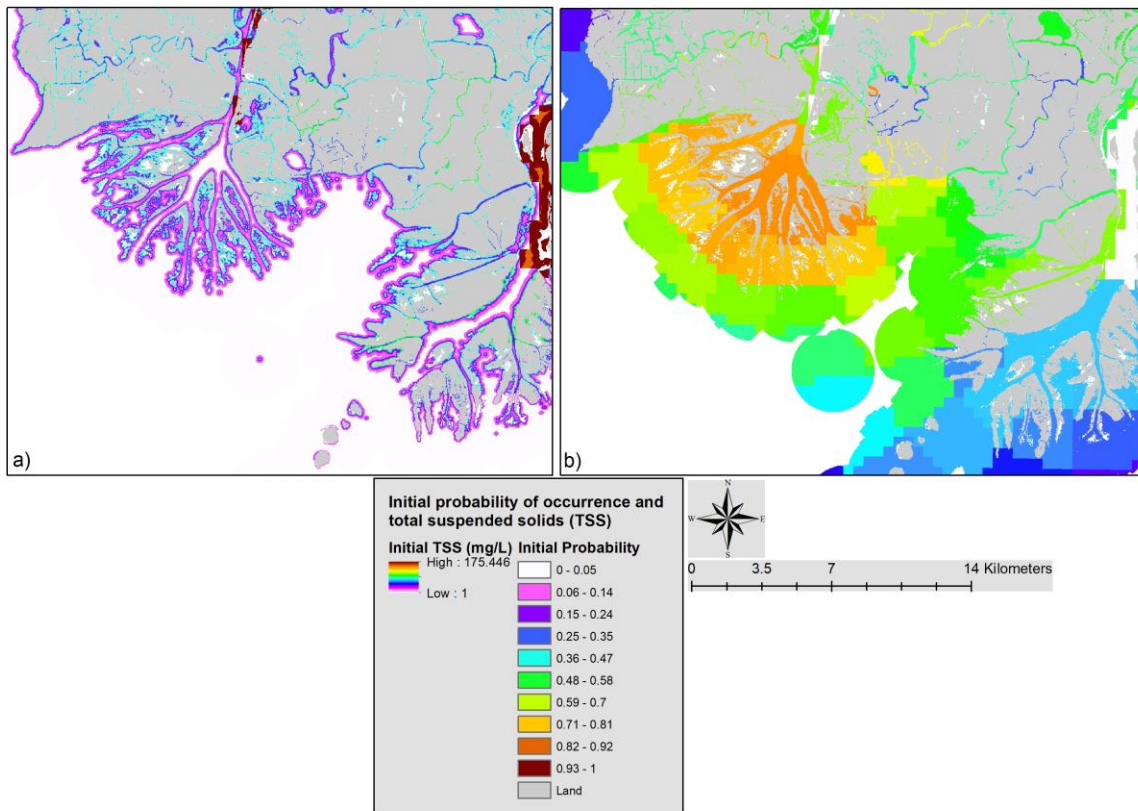
Figure 15. Initial Conditions (Y02) Probability of SAV Occurrence (a) and Modeled Total Suspended Solids (b) in the Wax Lake and Atchafalaya River Outflow Areas.

5.0 REFERENCES

Adams, J.B., Smith, M.O., Gillespie, A.R., 1993. In: Pieters, C.M., Englert, P. (Eds.), Remote Geochemical Analysis: Elemental and Mineralogical Composition. Cambridge University Press, New York, pp. 145–166

Cho, H. J., and Biber, P. D. (2016). Habitat characterization for submerged and floating-leaved aquatic vegetation in coastal river Deltas of Mississippi and Alabama. Southeastern Geographer 54 (4): 454-472.

Coastal Protection and Restoration Authority (CPRA), 2021. Coastwide Reference Monitoring System (CRMS) Data. Retrieved from Coastal Information Management System (CIMS) database. https://cims.coastal.louisiana.gov. August 2021.

Couvillion, B. R. (2021). Coastal wetland area change in the Gulf of Mexico, 1985-2020: U.S. Geological Survey data release, https://doi.org/10.5066/P9ZQI7ZW.

DeMarco, K., Couvillion, B., Brown, S., and La Peyre, M. (2018). Submerged aquatic vegetation mapping in coastal Louisiana through development of a spatial likelihood occurrence (SLOO) model. Aquatic Botany 151: 87-97. https://doi.org/10.1016/j.aquabot.2018.08.007.

DeMarco, K., Hillmann, E.R., Nyman, J.A., Couvillion, B., and La Peyre, M.K. 2021. Defining aquatic habitat zones across northern Gulf of Mexico estuarine gradients through submerged aquatic vegetation species assemblage and biomass data. Estuaries and Coast: https://doi.org/10.1007/s12237-021-00958-7

Doyle, R. D. and Smart, R. M. (2001). Impacts of water column turbidity on the survival and growth of Vallisneria americana winterbuds and seedlings. Lake and Reservoir Management 17 (1), 17-28.

Fonseca, M. and Bell, S. (1998). Influence of physical setting on seagrass landscapes near Beaufort, North Carolina. Marine Ecology Progress Series 121, 109-121.

Global Ocean Data Assimilation Experiment (GODAE), 2021. Hybrid Coordinate Ocean model (HYCOM) data. Retrieved from Google Earth Engine database. https://code.earthengine.google.com/ee.ImageCollection. (Accessed 12 October 2021)

Gracia, A. C., Rangel-Buitrago, N., Oakley, J. A., and Williams, A. (2017). Use of ecosystems in coastal erosion management. Ocean and Coastal Management: 1-17.

Gurbisz, C., Kemp, W. M., Sanford, L. P., and Orth, R. J. (2016). Mechanisms of storm-related loss and resilience in a large submersed plant bed. Estuaries and Coasts 39, 951-966.

Hillmann, E. R., DeMarco, K. E., and La Peyre, M. K. (2019). Salinity and water clarity dictate seasonal variability in coastal submerged aquatic vegetation in subtropical estuarine environments.

Aquatic Biology 28: 175-186.

Holm, G. A. Jr. and Sasser, C. E. (2001). Differential salinity response between two Mississippi River subdeltas: implications for changes in plant composition. Estuaries 24 (1): 78-89.

Jarvis, J. C. and Moore, K. A. (2008). Influence of environmental factors on Vallisneria americana seed germination. Aquatic Botany 88, 283-294.

Jensen, D., Simard, M., Cavanaugh, K., Sheng, Y., Fichot, C. G., Pavelsky, T., Twilley, R. (2019). Improving the Transferability of Suspended Solid Estimation in Wetland and Deltaic Waters with an Empirical Hyperspectral Approach. Remote Sensing. 11 (13):1629. https://doi.org/10.3390/rs11131629

Juston, J. M., DeBusk, T. A., Grace, K. A., and Jackson, S. D. (2013). A model of phosphorus cycling to explore the role of biomass turnover in submerged aquatic vegetation wetlands for Everglades restoration. Ecological Modeling 251: 135-149.

Kinney, E. L., Quigg, A., and Armitage, A. R. (2014). Acute effects of drought on emergent and aquatic communities in a brackish marsh. Estuaries and Coasts 37: 636-645.

Kolker, A. S., Bargu, S., Brenner, J., Chu, P., Conover, J., De Mutsert, K., Fitzpatrick, C., Greenhow, D. Justic, D., Lohrenz, S., Montagna, P., Snider Peyronnin, N., Proville, J., Renfro, A., Rhode, R., Roberts, B., Taylor, C. Wade, T., Walker, N., and Wallace, D. (2018). The impacts of the Mississippi River and its delta on the oceanography, ecology, and economy of the Gulf of Mexico large marine ecosystem. Restore the Mississippi River Delta, white paper: http://mississippiriverdelta.org/learning/impacts-of-the-mississippi-river/

Ng, A. Y. and Jordan, M. I. (2001) On discriminative vs. generative classifiers: a comparison of logistic regression and naive Bayes. In: Dietterich TG, Becker S, Ghahramani Z (eds) NIPS. MIT Press, MA, pp 841–848.

Pulich, W. M. and White, W. A. (1991). Decline of submerged vegetation in the Galveston Bay system: chronology and relationships to physical processes. Journal of Coastal Research 7 (4), 1125-1138.

R Core Team (2021). R: A language and environment for statistical computing. R Foundation for Statistical Computing, Vienna, Austria. URL: https://www.R-project.org/.

Robbins, B. D. and Bell, S. S. (2000). Dynamics of a subtidal seagrass landscape: seasonal and annual change in relation to water depth. Ecology 81 (5), 1193-1205.

Roberts, D.A., Smith, M.O., Adams, J.B., 1993. Green vegetation, nonphotosynthetic ve-

getation, and soils in AVIRIS data. Remote Sens. Environ. 44, 255–269. https://doi.

org/10.1016/0034-4257(93)90020-X.

Santos, R. O., Lirman, D., and Serafy, J. E. (2011). Quantifying freshwater-induced fragmentation of submerged aquatic vegetation communities using a multi-scale landscape ecology approach. Marine Ecology Progress Series 427, 233-246.

Settle, J.J., Drake, N.A., 1993. Linear mixing and the estimation of ground cover pro-portions. Int. J. Remote Sens. 14, 1159–1177. https://doi.org/10.1080/01431169308904402

Strasizar, T., Koch, M. S., Madden, C. J., Filina, J., Lara, P. U., and Mattair, A. (2013). Salinity effects on Ruppia maritima L. seed germination and seedling survival at the Everglades-Florida Bay ecotone. Journal of Experimental Marine Biology and Ecology 445, 129-139.

Swam, L.A., Couvillion, B., Callam, B., La Peyre, J.K., and La Peyre, M. (2022). Defining oyster resource zones across coastal Louisiana for restoration and aquaculture,Ocean & Coastal Management,Volume 225, ISSN 0964-5691,https://doi.org/10.1016/

United States Geological Survey (USGS) of US Department of the Interior, 2021. USGS Current Condition for the Nation. Retrieved from National Water Information System: Web Interface. https://nwis.waterdata.usgs.gov/usa/nwis/uv/?. (Accessed 23 August 2021).

Västilä, K. and Järvelä, J. (2017). Characterizing natural riparian vegetation for modeling of flow and suspended sediment transport. Journal of Soils and Sediments: DIO 10.1007/s11368-017-1776-3.

Yan, Z., Song, B., Zhang, L., Liu, M., Liu, Y., Wu, X., Tian, Y., Chen, Z., and Zhao, J. (2016). Effects of Submerged Plants on the Growth of Eutrophic Algae and Nutrient Removal in Constructed Wetlands. Open Access Library Journal 3: e3056. http://dx.doi.org/10.4236/oalib.1103056

APPENDIX 1: FREQUENCY OF DETECTION OF SAV GRIDDED MAPS

Frequency of SAV Detection (2015-2018)

- 1%-33% of observations
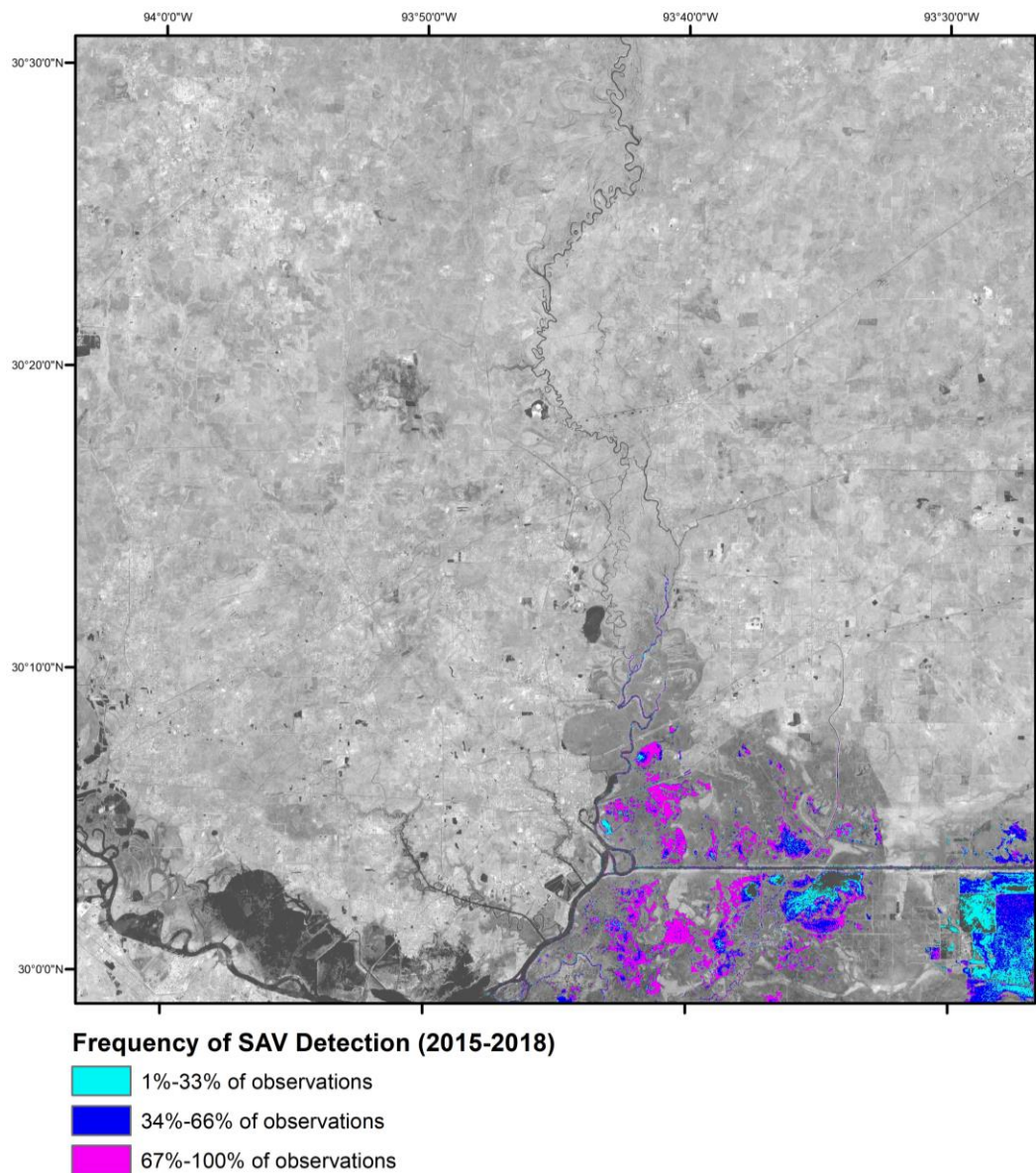- 34%-66% of observations
- 67%-100% of observations

Figure A1. Visualization of the Frequency of SAV Detection layer in a 30'x30' cell from approximately 30.5°N to 30°N and 94°W to 93.5°W.

Frequency of SAV Detection (2015-2018)

- 1%-33% of observations
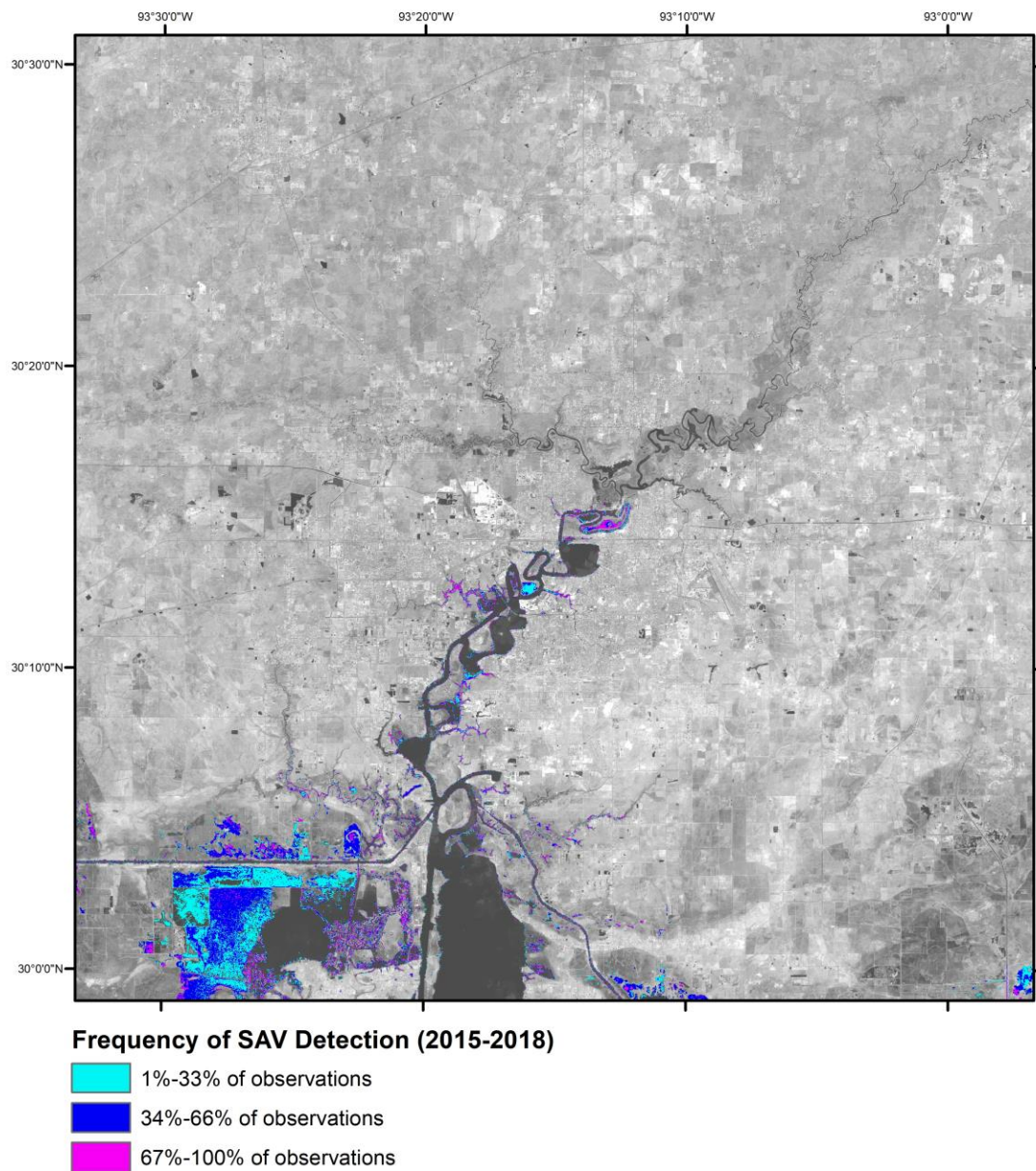- 34%-66% of observations
- 67%-100% of observations

Figure A2. Visualization of the Frequency of SAV Detection layer in a 30'x30' cell from approximately 30.5°N to 30°N and 93.5°W to 93.0°W.

Frequency of SAV Detection (2015-2018)

- ■ 1%-33% of observations
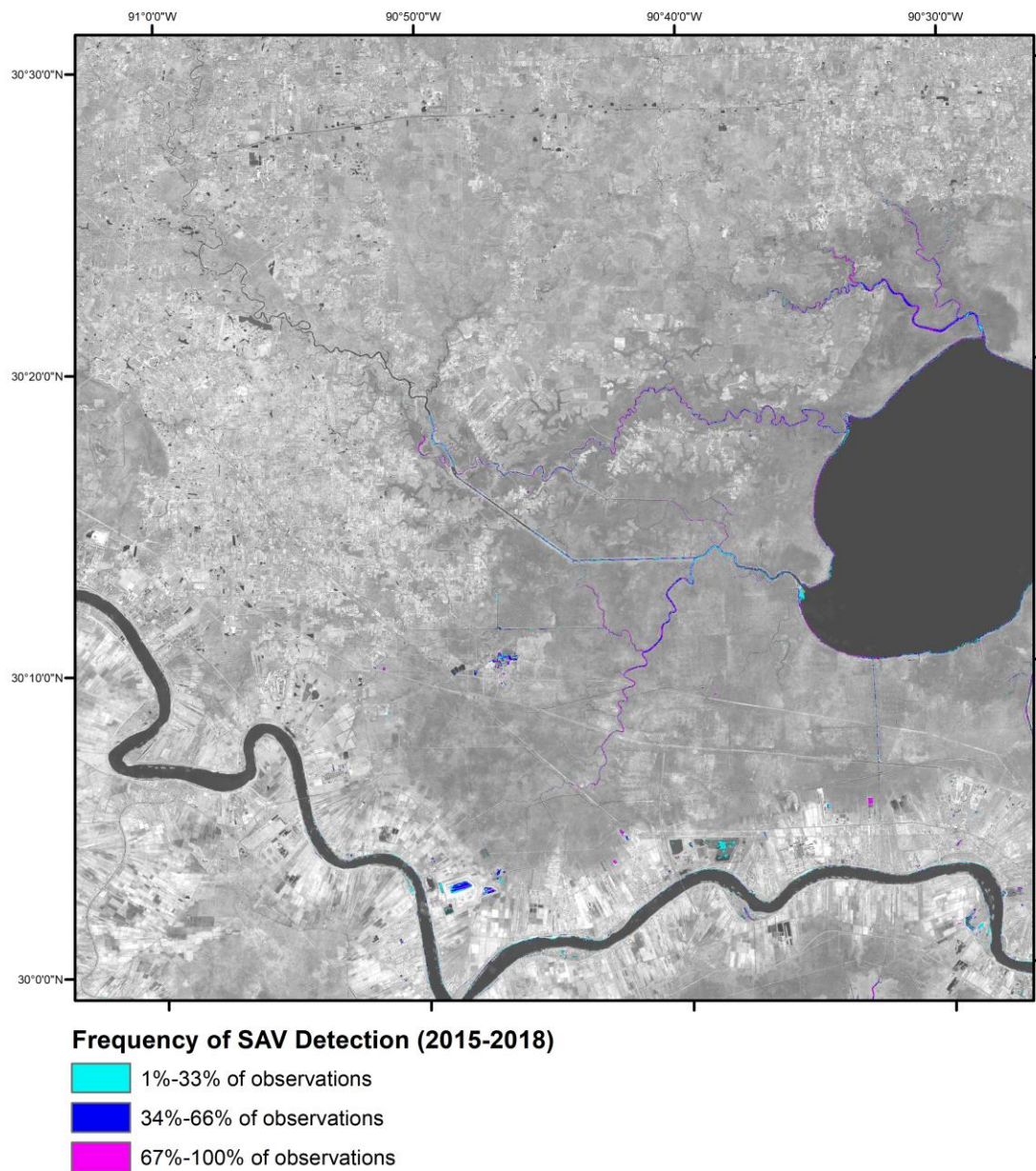- ■ 34%-66% of observations
- ■ 67%-100% of observations

Figure A3. Visualization of the Frequency of SAV Detection layer in a 30'x30' cell from approximately 30.5°N to 30°N and 91°W to 90.5°W.

Frequency of SAV Detection (2015-2018)

- 1%-33% of observations
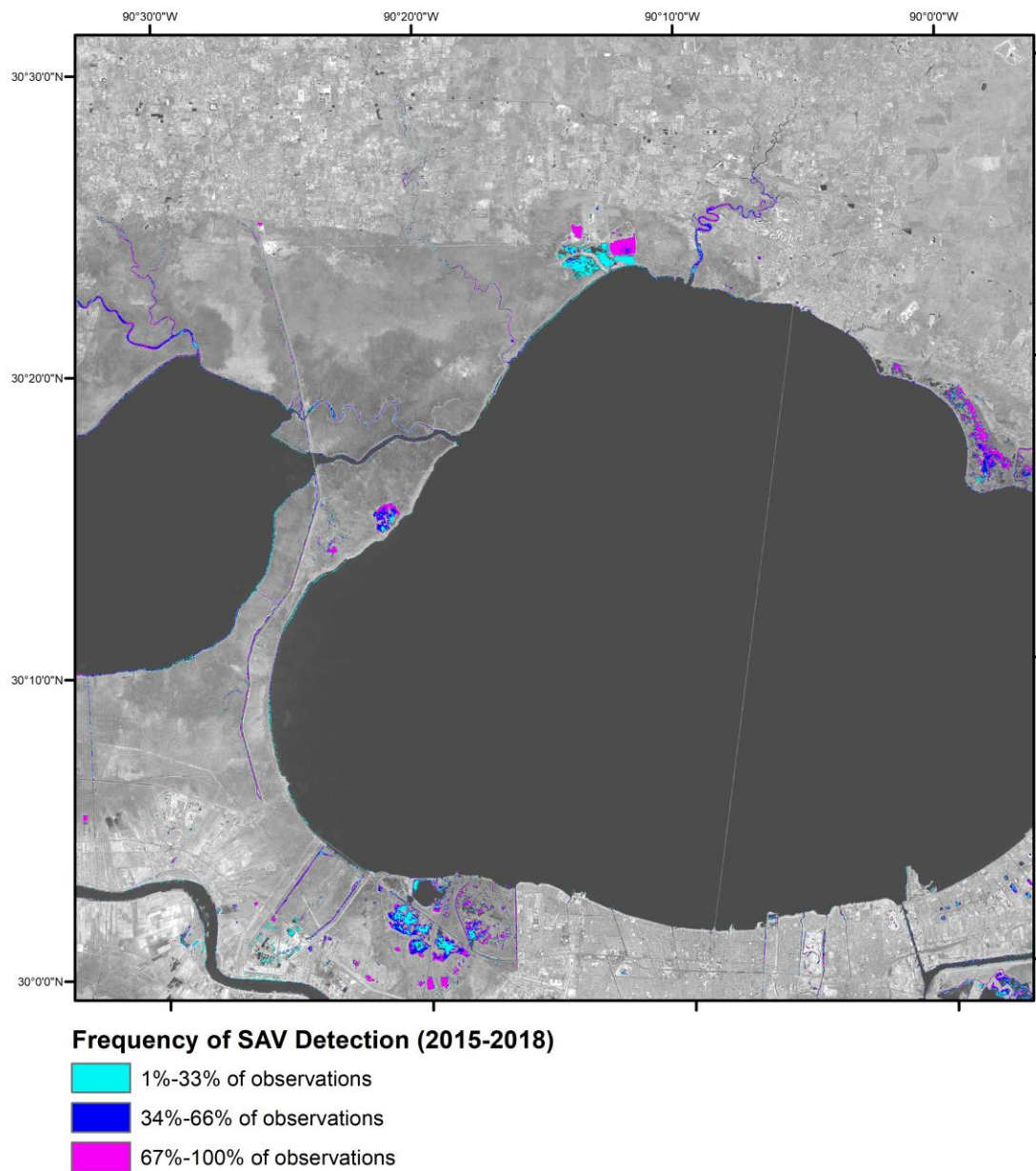- 34%-66% of observations
- 67%-100% of observations

Figure A4. Visualization of the Frequency of SAV Detection layer in a 30'x30' cell from approximately 30.5°N to 30°N and 90.5°W to 90°W.

Frequency of SAV Detection (2015-2018)

- 1%-33% of observations
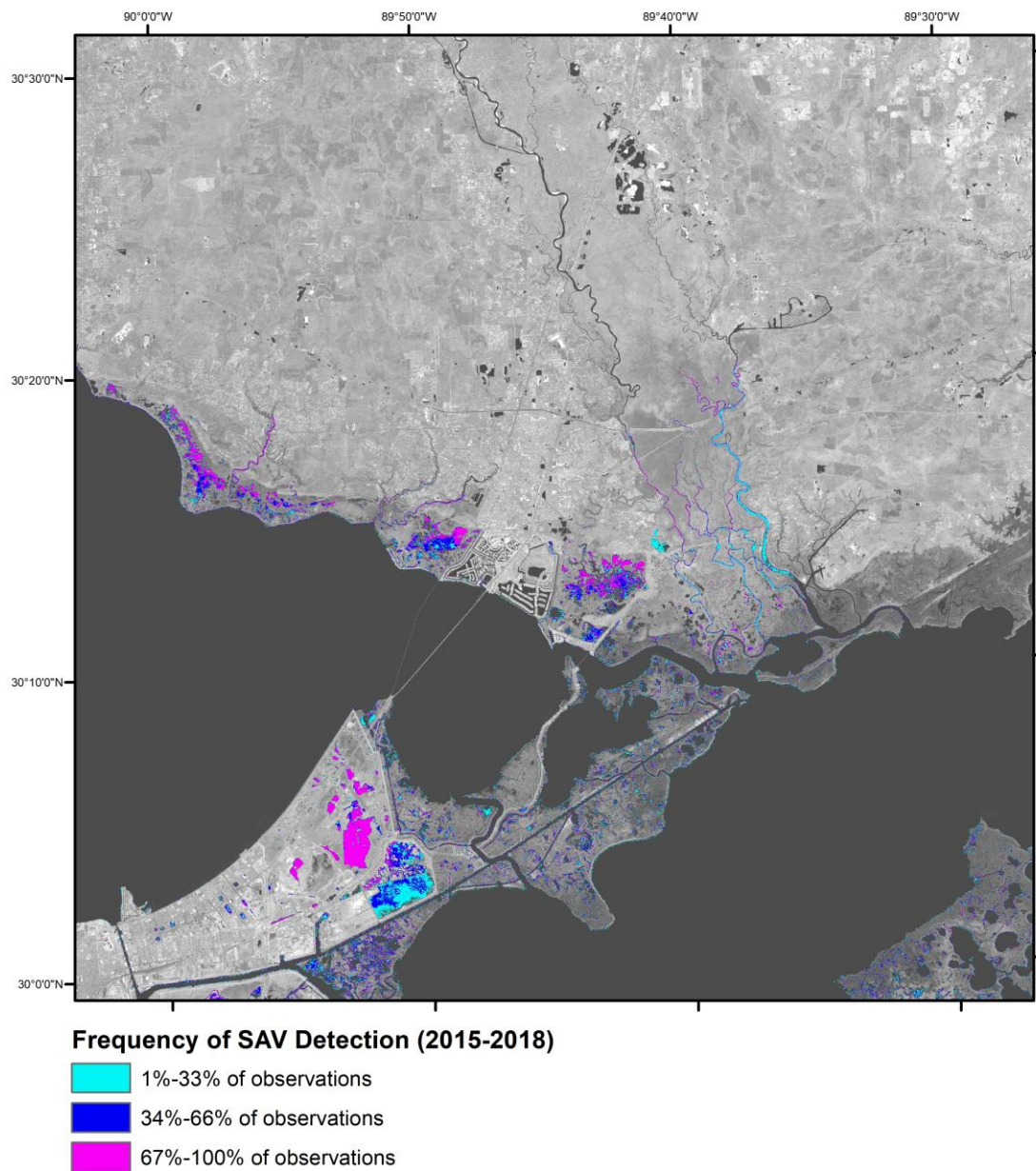- 34%-66% of observations
- 67%-100% of observations

Figure A5. Visualization of the Frequency of SAV Detection layer in a 30'x30' cell from approximately 30.5°N to 30°N and 90°W to 89.5°W.

Frequency of SAV Detection (2015-2018)

- 1%-33% of observations
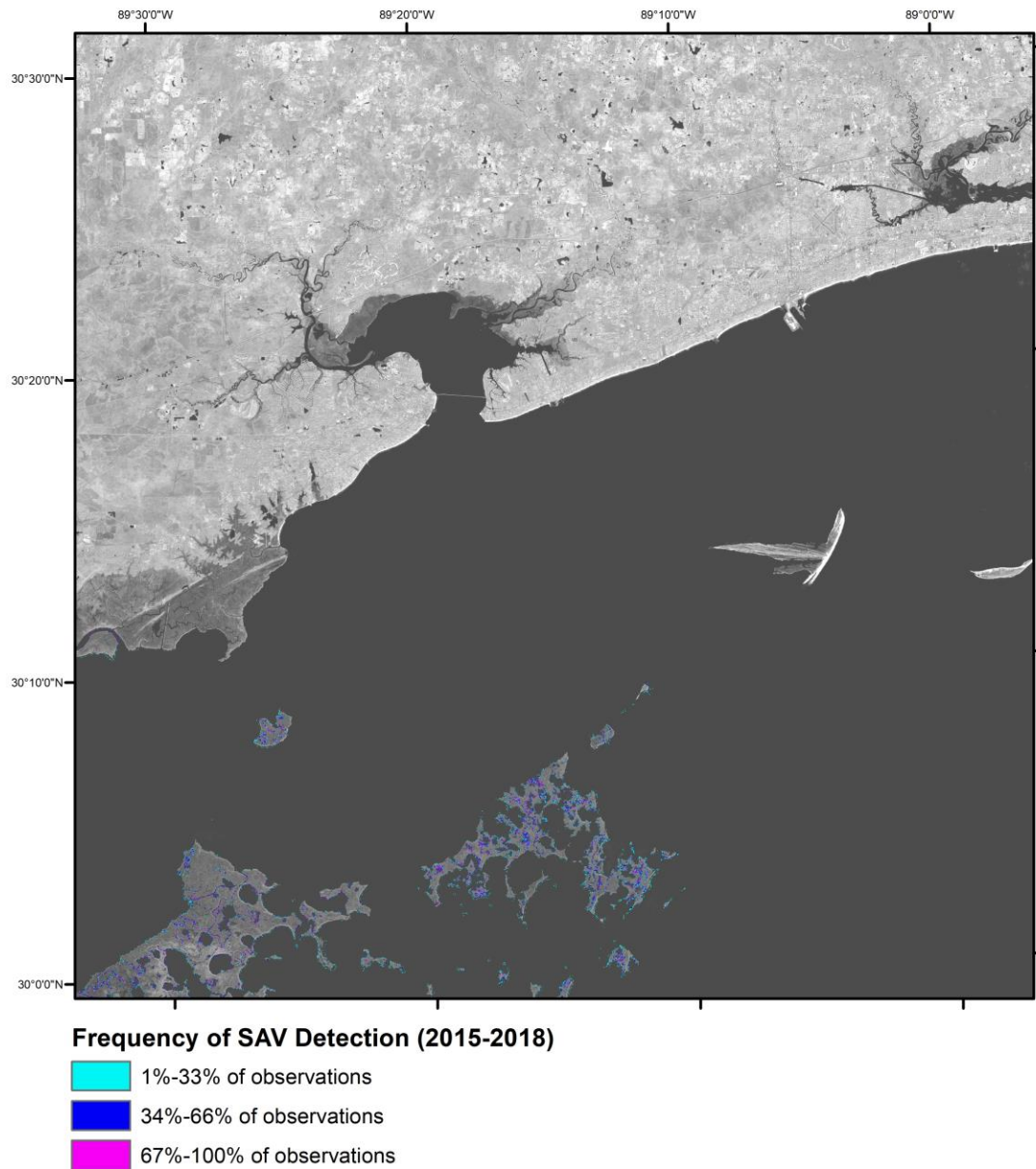- 34%-66% of observations
- 67%-100% of observations

Figure A6. Visualization of the Frequency of SAV Detection layer in a 30'x30' cell from approximately 30.5°N to 30°N and 89.5°W to 89°W.

Frequency of SAV Detection (2015-2018)
- 1%-33% of observations
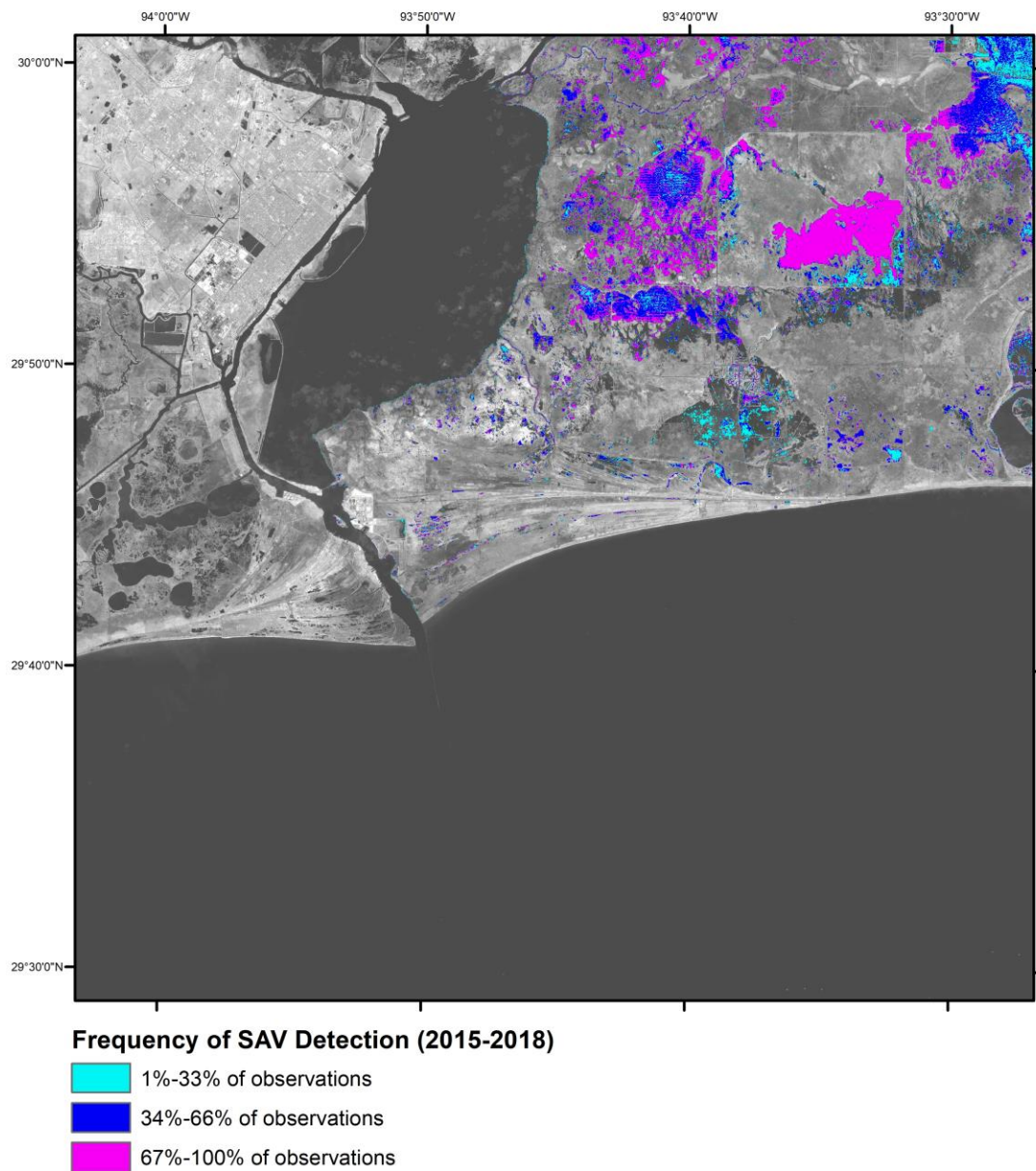- 34%-66% of observations
- 67%-100% of observations

Figure A7. Visualization of the Frequency of SAV Detection layer in a 30'x30' cell from approximately 30°N to 29.5°N and 94°W to 93.5°W.

Frequency of SAV Detection (2015-2018)

- 1%-33% of observations
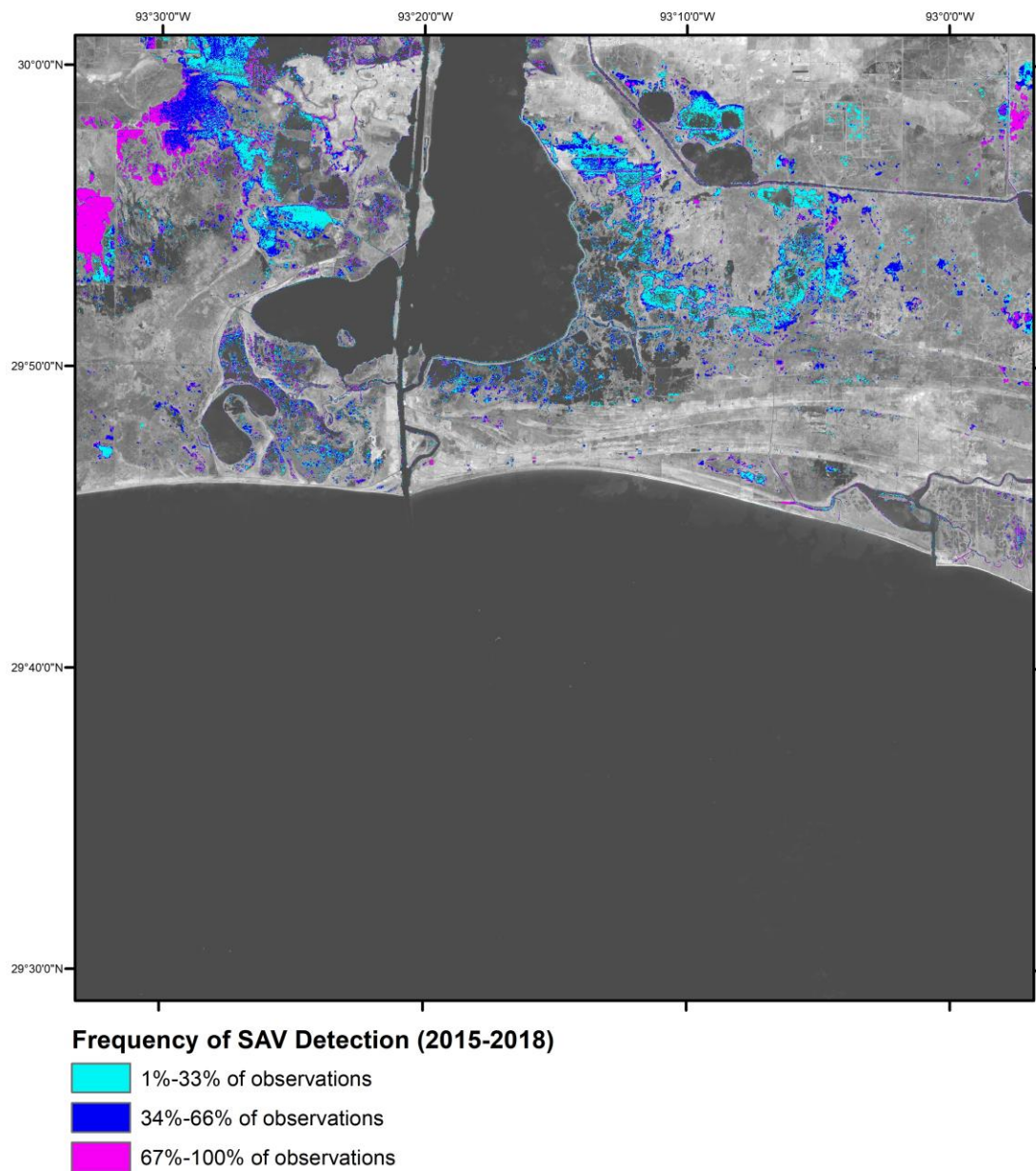- 34%-66% of observations
- 67%-100% of observations

Figure A8. Visualization of the Frequency of SAV Detection layer in a 30'x30' cell from approximately 30°N to 29.5°N and 93.5°W to 93°W.

Frequency of SAV Detection (2015-2018)

- 1%-33% of observations
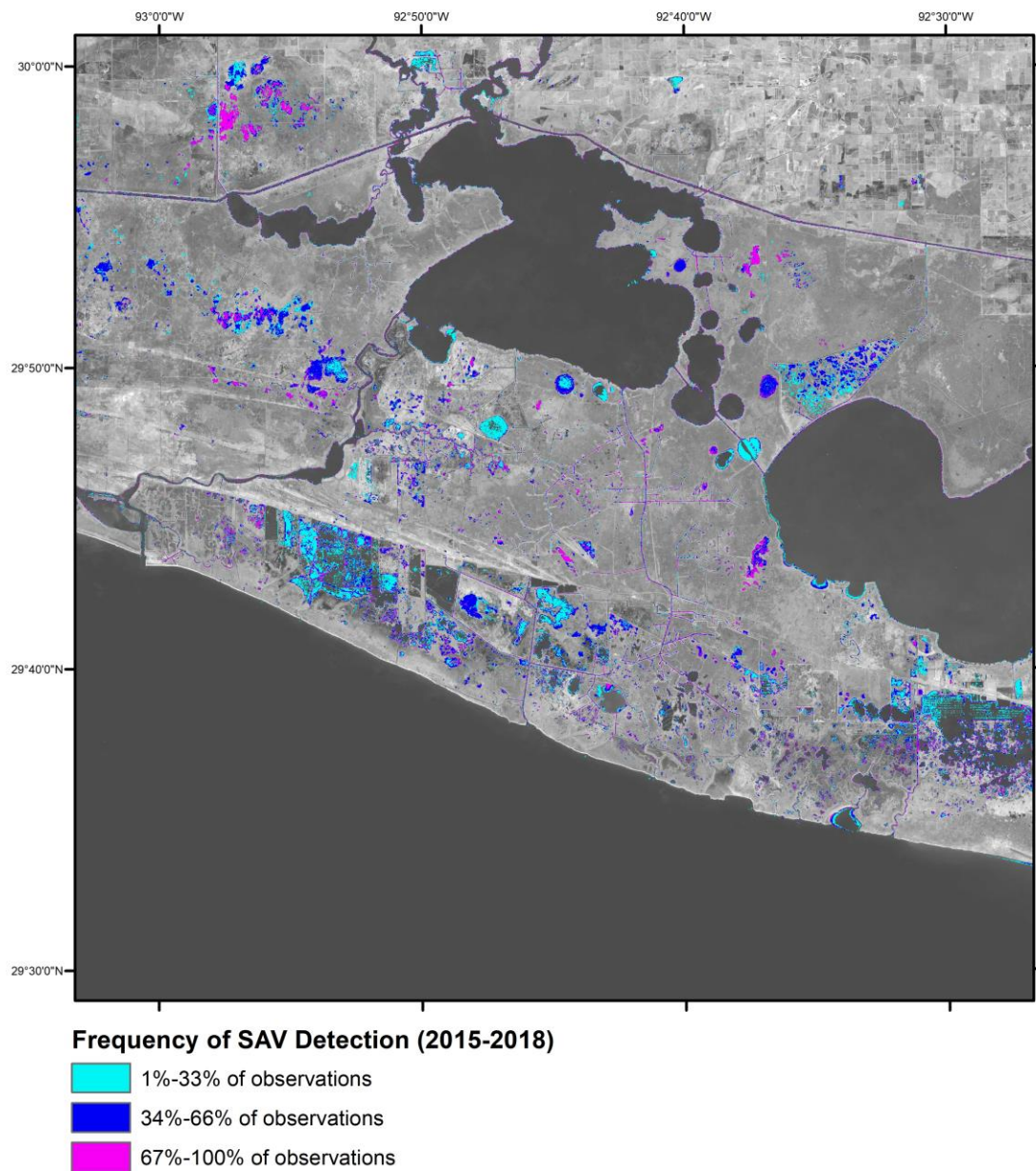- 34%-66% of observations
- 67%-100% of observations

Figure A9. Visualization of the Frequency of SAV Detection layer in a 30'x30' cell from approximately 30°N to 29.5°N and 93°W to 92.5°W.

Frequency of SAV Detection (2015-2018)

■ 1%-33% of observations
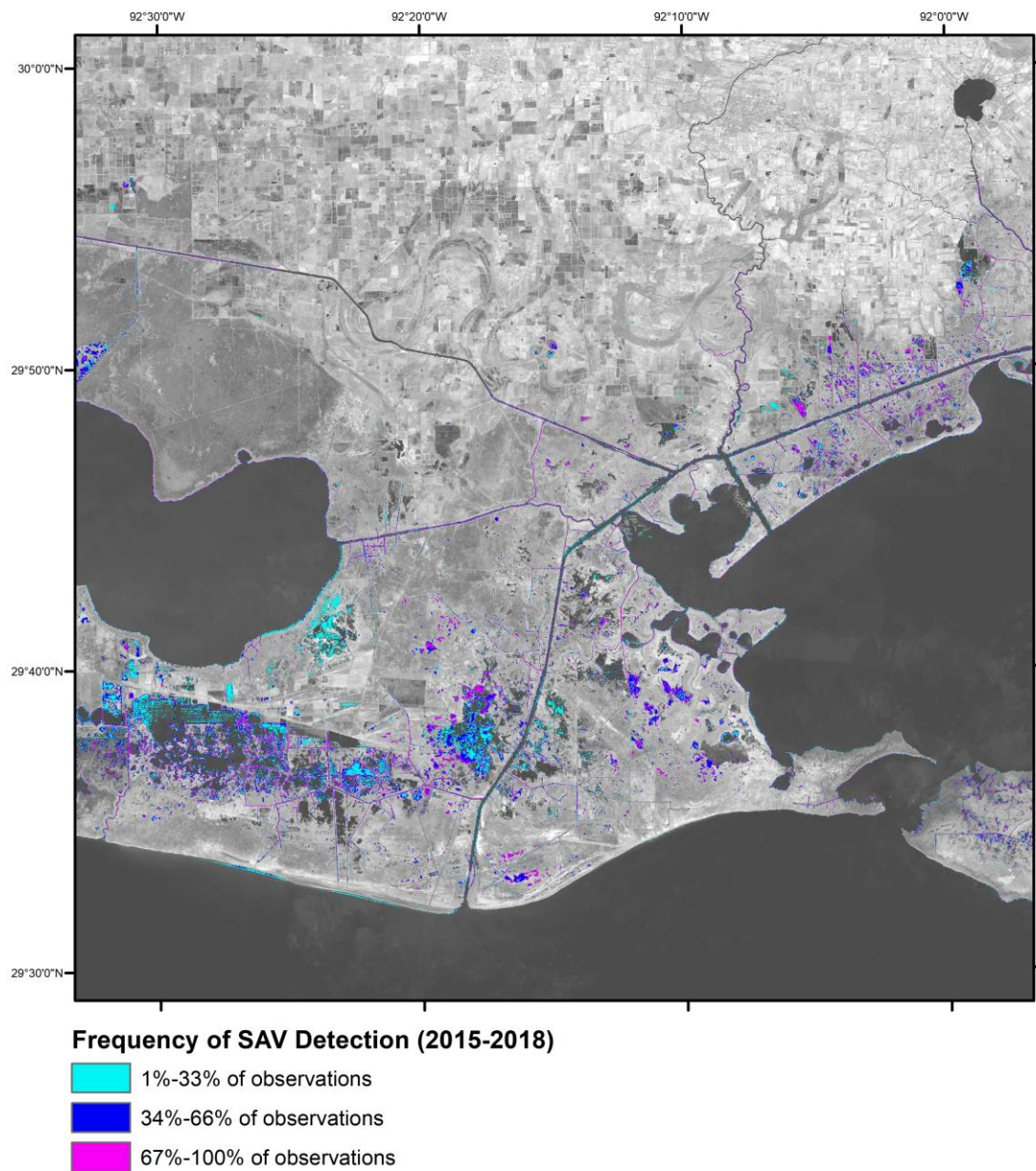■ 34%-66% of observations
■ 67%-100% of observations

Figure A10. Visualization of the Frequency of SAV Detection layer in a 30'x30' cell from approximately 30°N to 29.5°N and 92.5°W to 92°W.

Frequency of SAV Detection (2015-2018)

- 1%-33% of observations
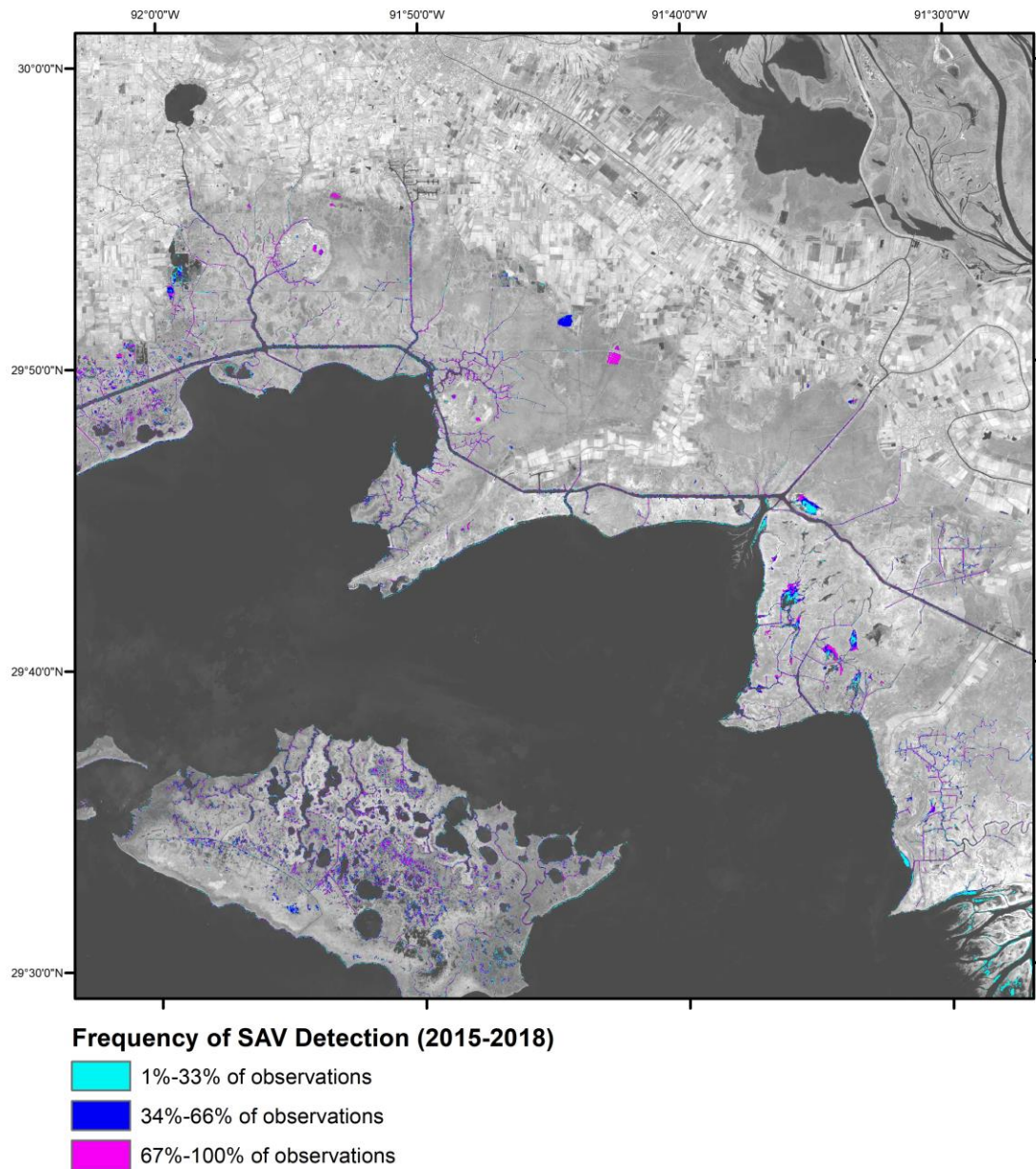- 34%-66% of observations
- 67%-100% of observations

Figure A11. Visualization of the Frequency of SAV Detection layer in a 30'x30' cell from approximately 30°N to 29.5°N and 92°W to 91.5°W.

Frequency of SAV Detection (2015-2018)

- 1%-33% of observations
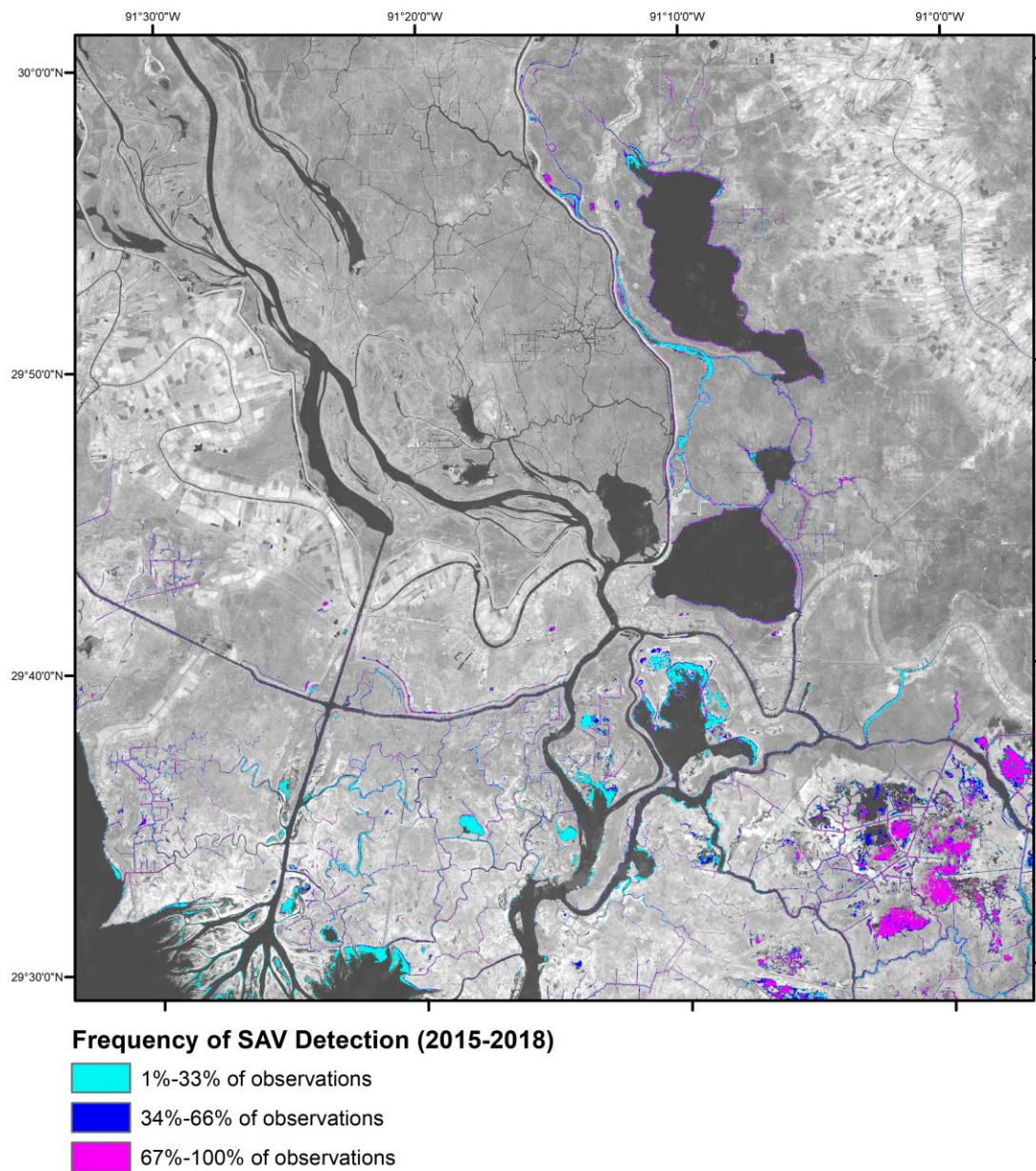- 34%-66% of observations
- 67%-100% of observations

Figure A12. Visualization of the Frequency of SAV Detection layer in a 30'x30' cell from approximately 30°N to 29.5°N and 91.5°W to 91°W.

Frequency of SAV Detection (2015-2018)

- ☐ 1%-33% of observations
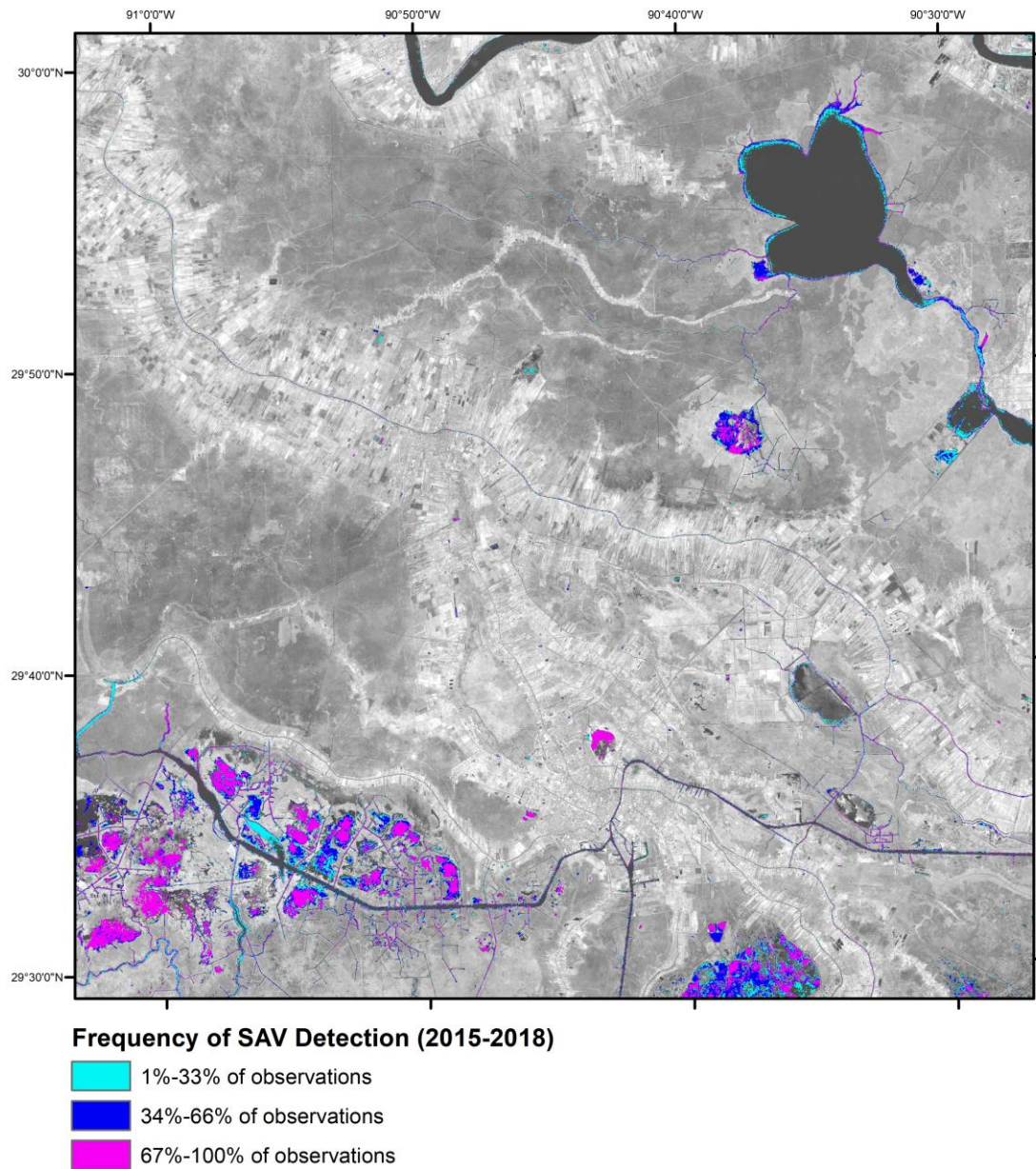- ☐ 34%-66% of observations
- ☐ 67%-100% of observations

Figure A13. Visualization of the Frequency of SAV Detection layer in a 30'x30' cell from approximately 30°N to 29.5°N and 91°W to 90.5°W.

Frequency of SAV Detection (2015-2018)

■ 1%-33% of observations
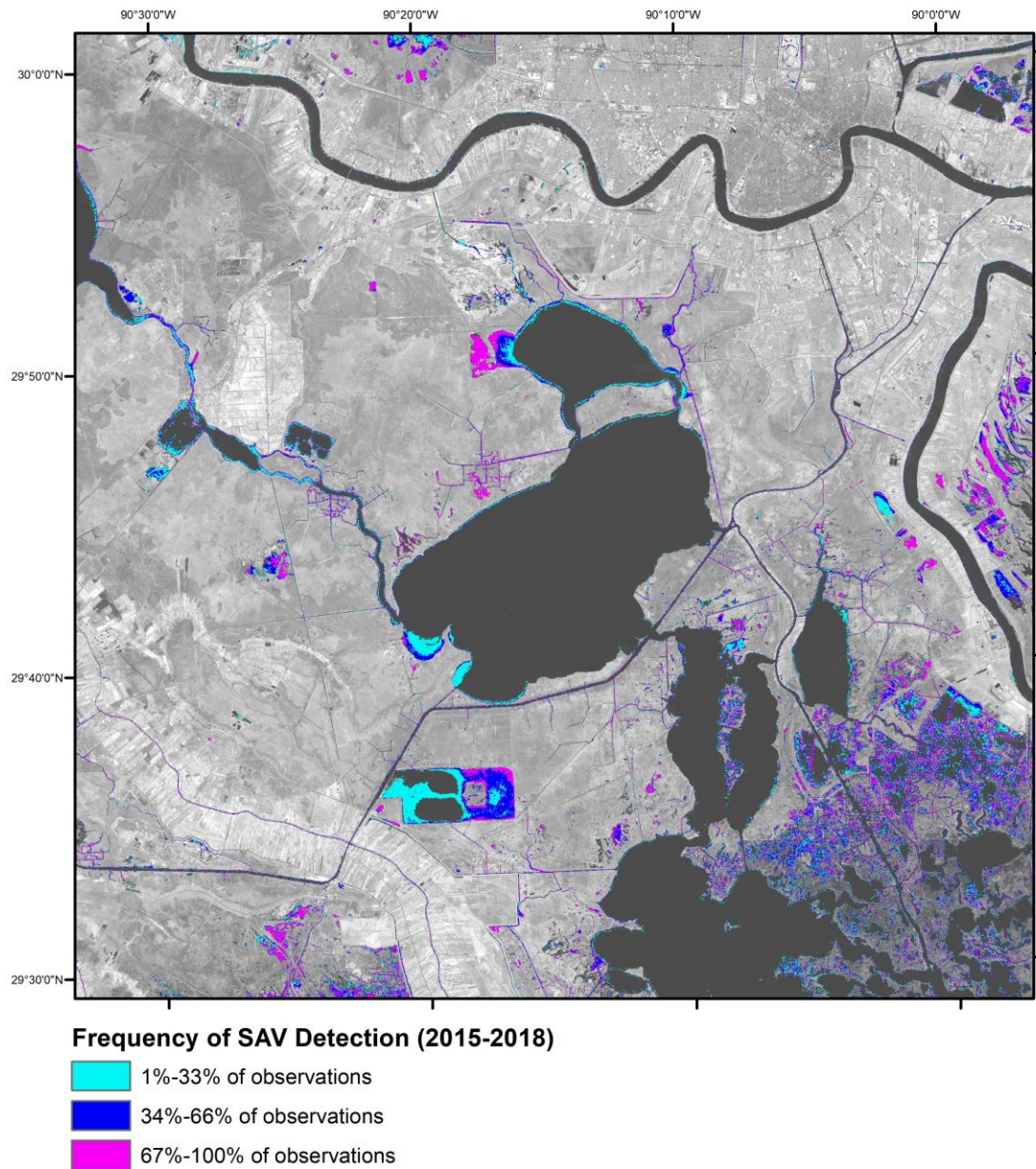■ 34%-66% of observations
■ 67%-100% of observations

Figure A14. Visualization of the Frequency of SAV Detection layer in a 30'x30' cell from approximately 30°N to 29.5°N and 90.5°W to 90°W.

Frequency of SAV Detection (2015-2018)

▭ 1%-33% of observations
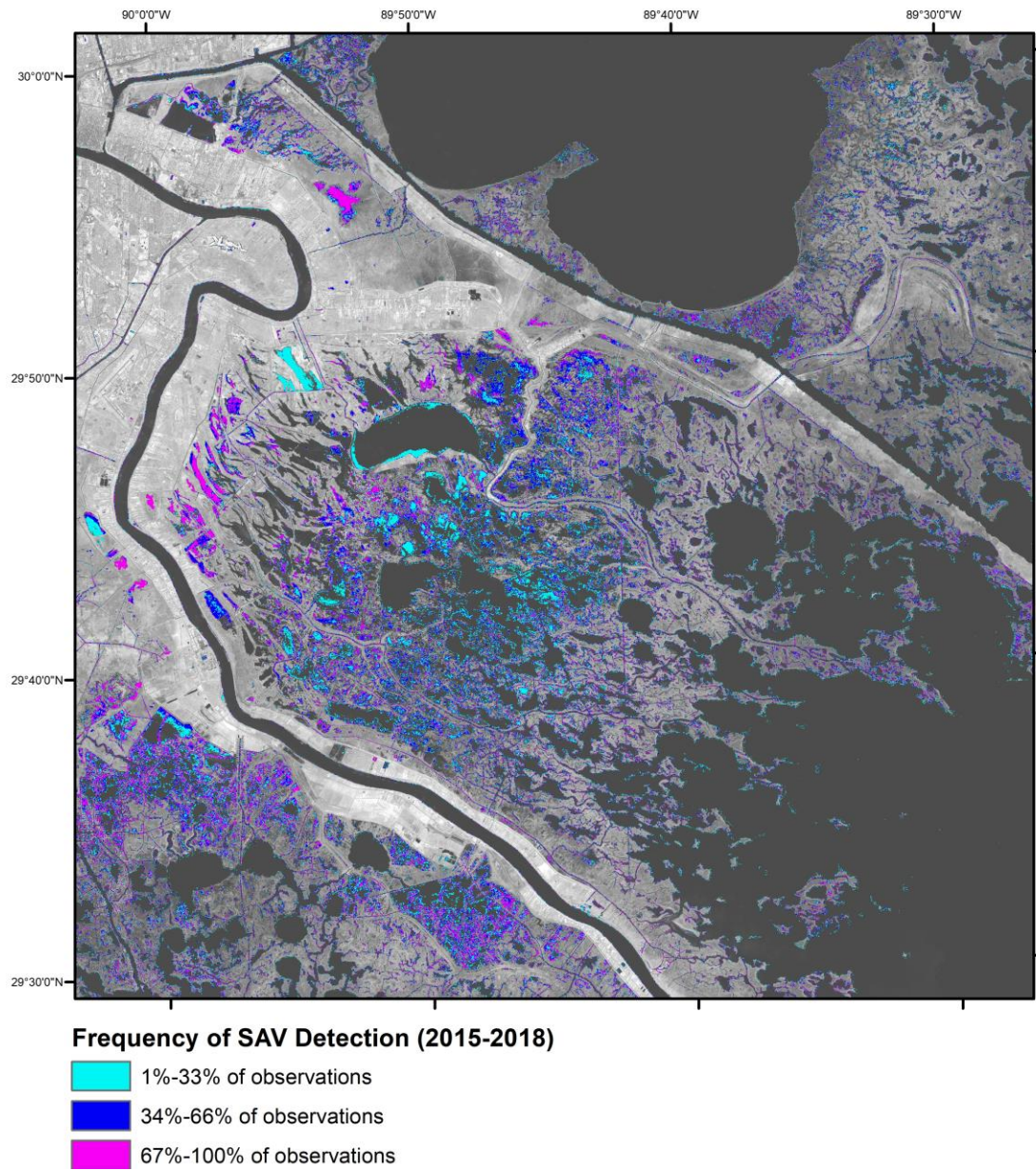
▭ 34%-66% of observations

▭ 67%-100% of observations

Figure A15. Visualization of the Frequency of SAV Detection layer in a 30'x30' cell from approximately 30°N to 29.5°N and 90°W to 89.5°W.

Frequency of SAV Detection (2015-2018)

- 1%-33% of observations
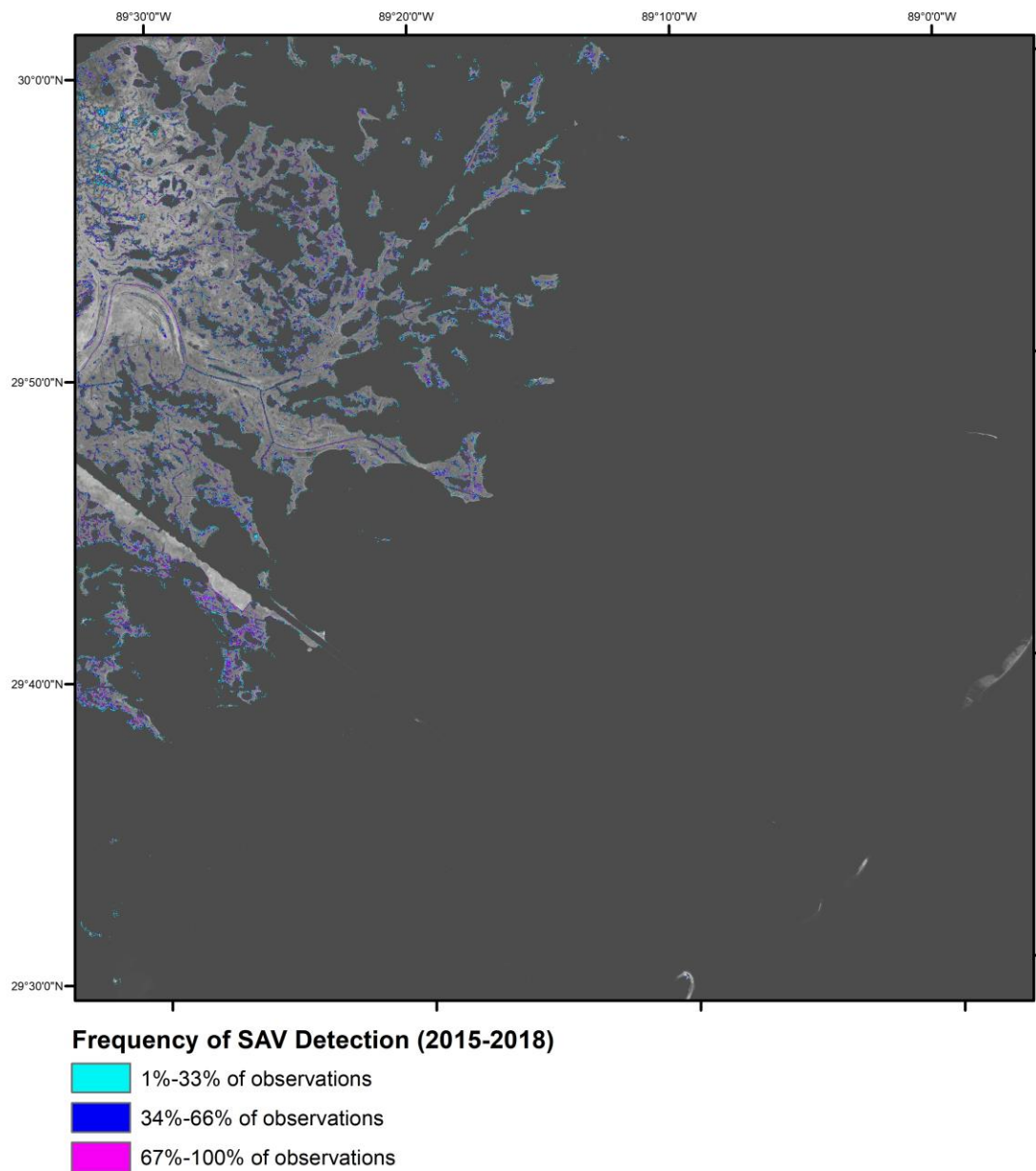- 34%-66% of observations
- 67%-100% of observations

Figure A16. Visualization of the Frequency of SAV Detection layer in a 30'x30' cell from approximately 30°N to 29.5°N and 89.5°W to 89°W.

Frequency of SAV Detection (2015-2018)

■ 1%-33% of observations
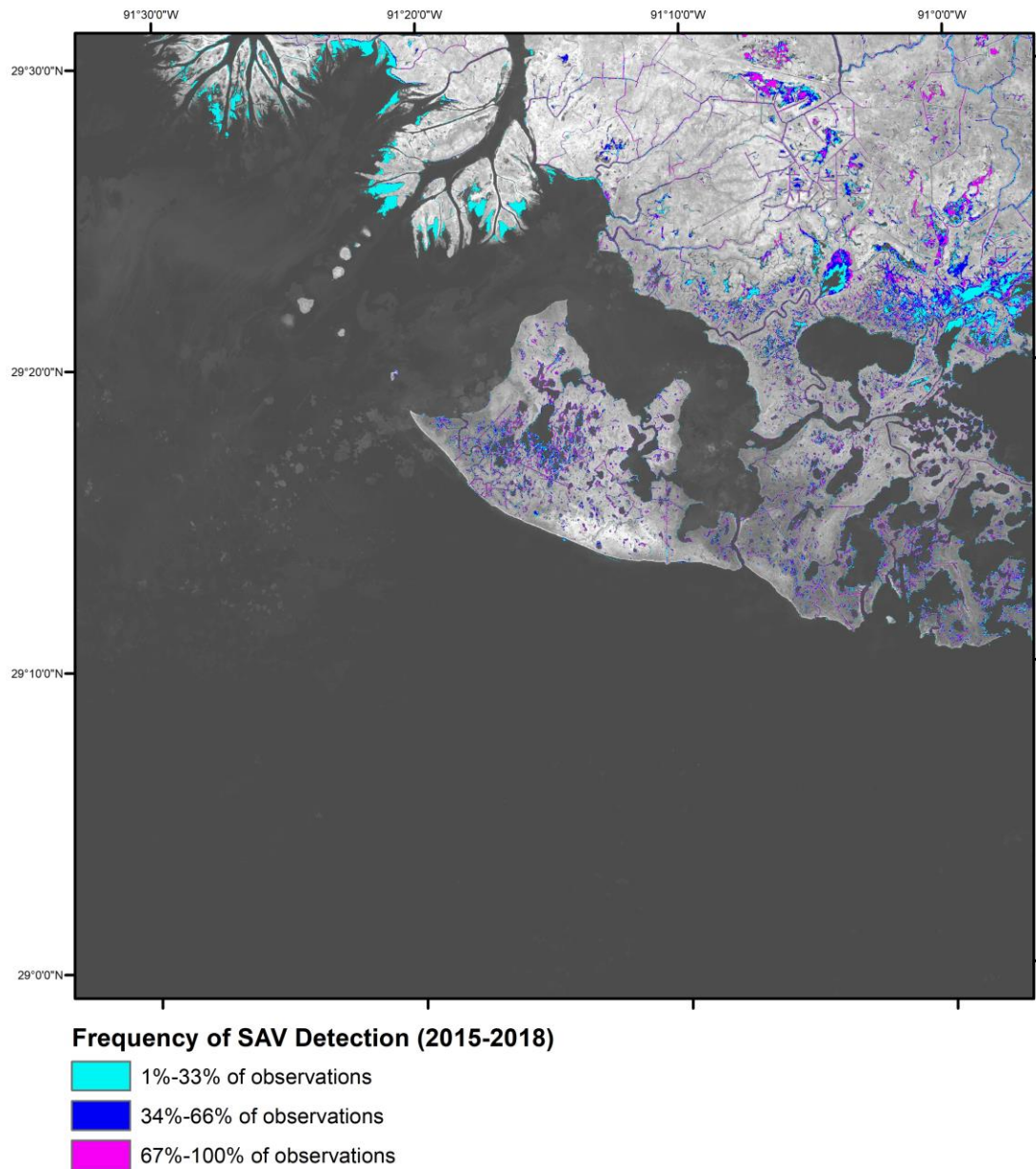
■ 34%-66% of observations

■ 67%-100% of observations

Figure A17. Visualization of the Frequency of SAV Detection layer in a 30'x30' cell from approximately 29.5°N to 29°N and 91.5°W to 91°W.

Frequency of SAV Detection (2015-2018)

- 1%-33% of observations
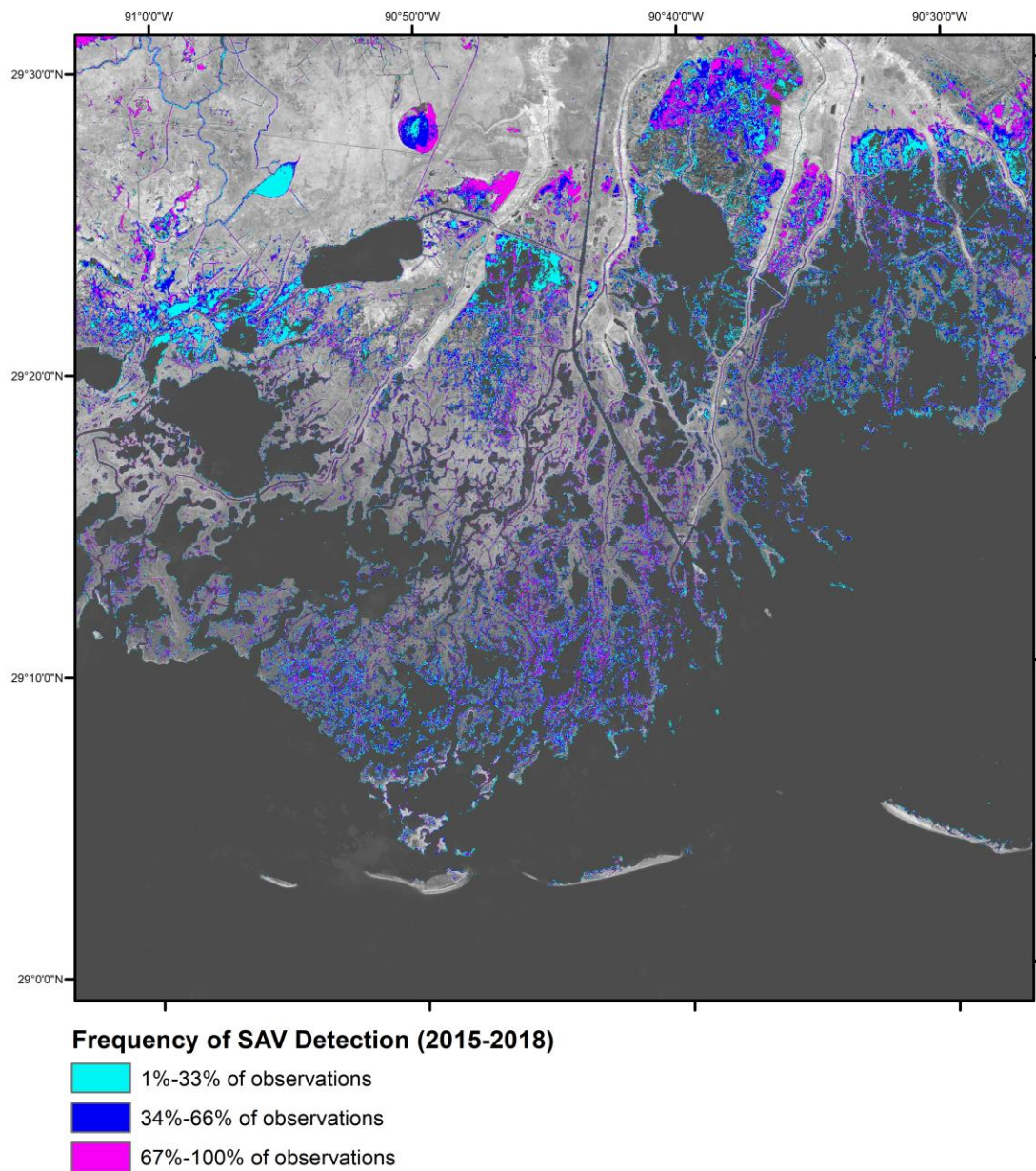- 34%-66% of observations
- 67%-100% of observations

Figure A18. Visualization of the Frequency of SAV Detection layer in a 30'x30' cell from approximately 29.5°N to 29°N and 91°W to 90.5°W.

Frequency of SAV Detection (2015-2018)

- ▢ 1%-33% of observations
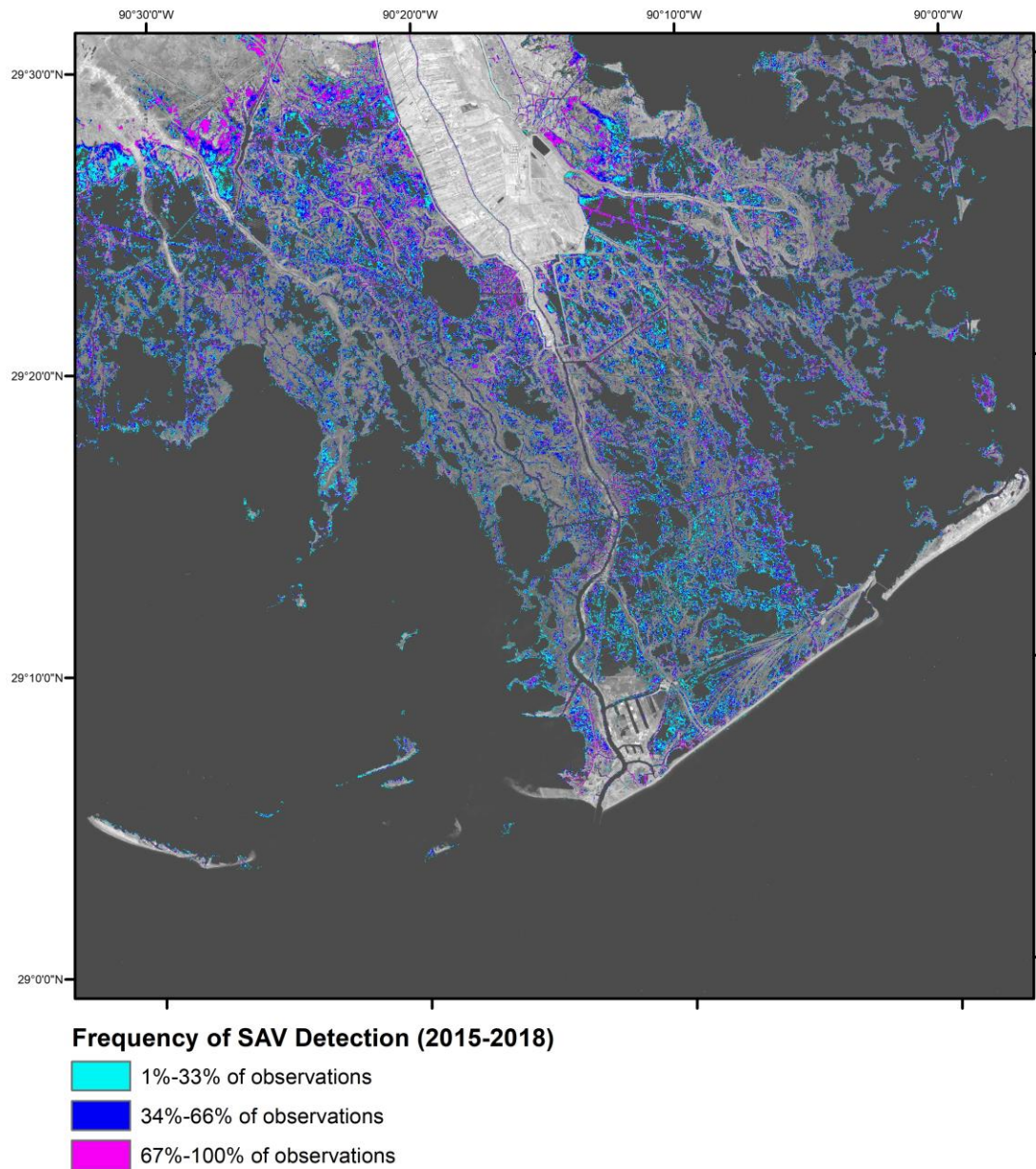- ▢ 34%-66% of observations
- ▢ 67%-100% of observations

Figure A19. Visualization of the Frequency of SAV Detection layer in a 30'x30' cell from approximately 29.5°N to 29°N and 90.5°W to 90°W.

Frequency of SAV Detection (2015-2018)

- ▨ 1%-33% of observations
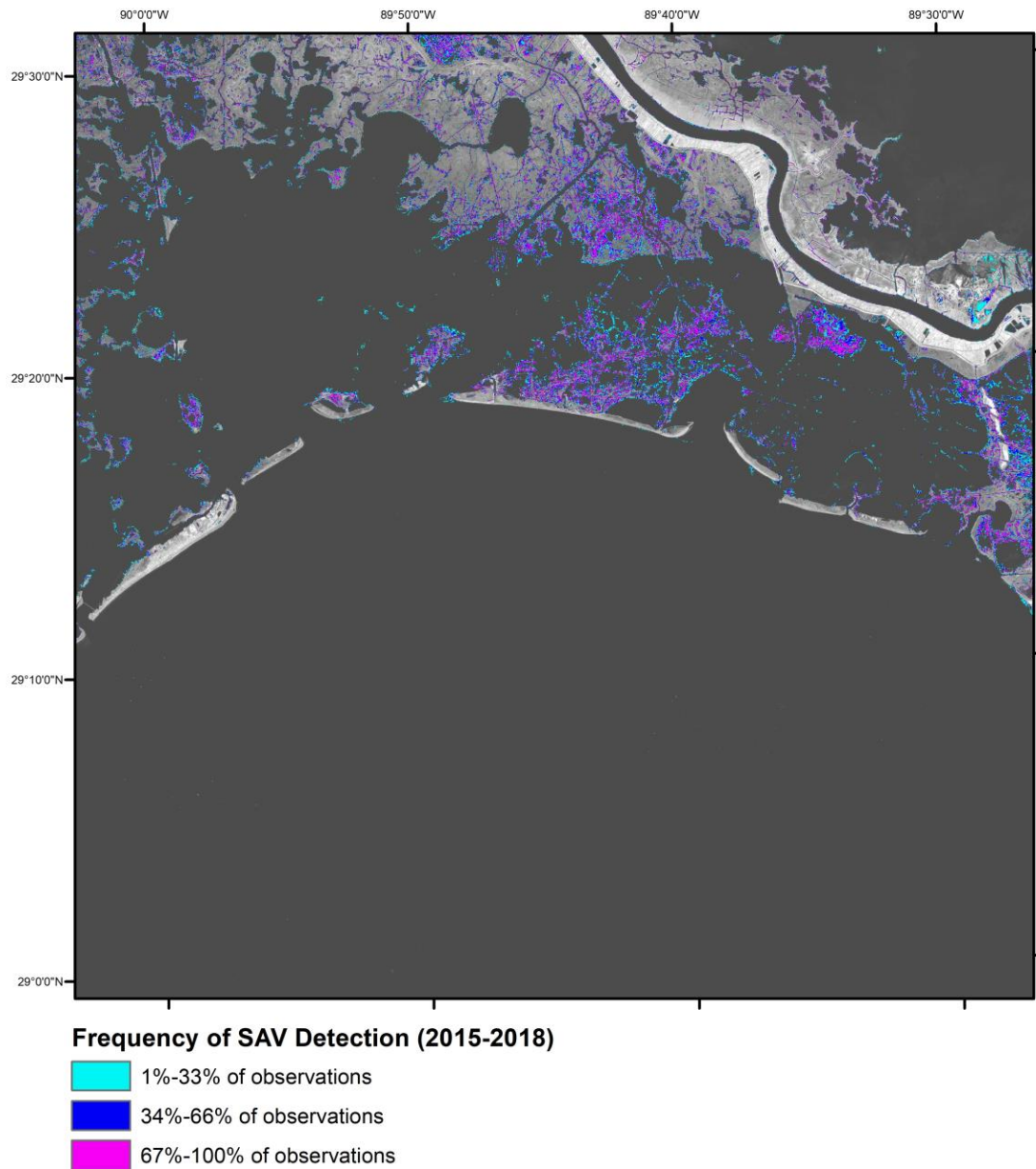- ▨ 34%-66% of observations
- ▨ 67%-100% of observations

Figure A20. Visualization of the Frequency of SAV Detection layer in a 30'x30' cell from approximately 29.5°N to 29°N and 90°W to 89.5°W.

Frequency of SAV Detection (2015-2018)

- 1%-33% of observations
- 34%-66% of observations
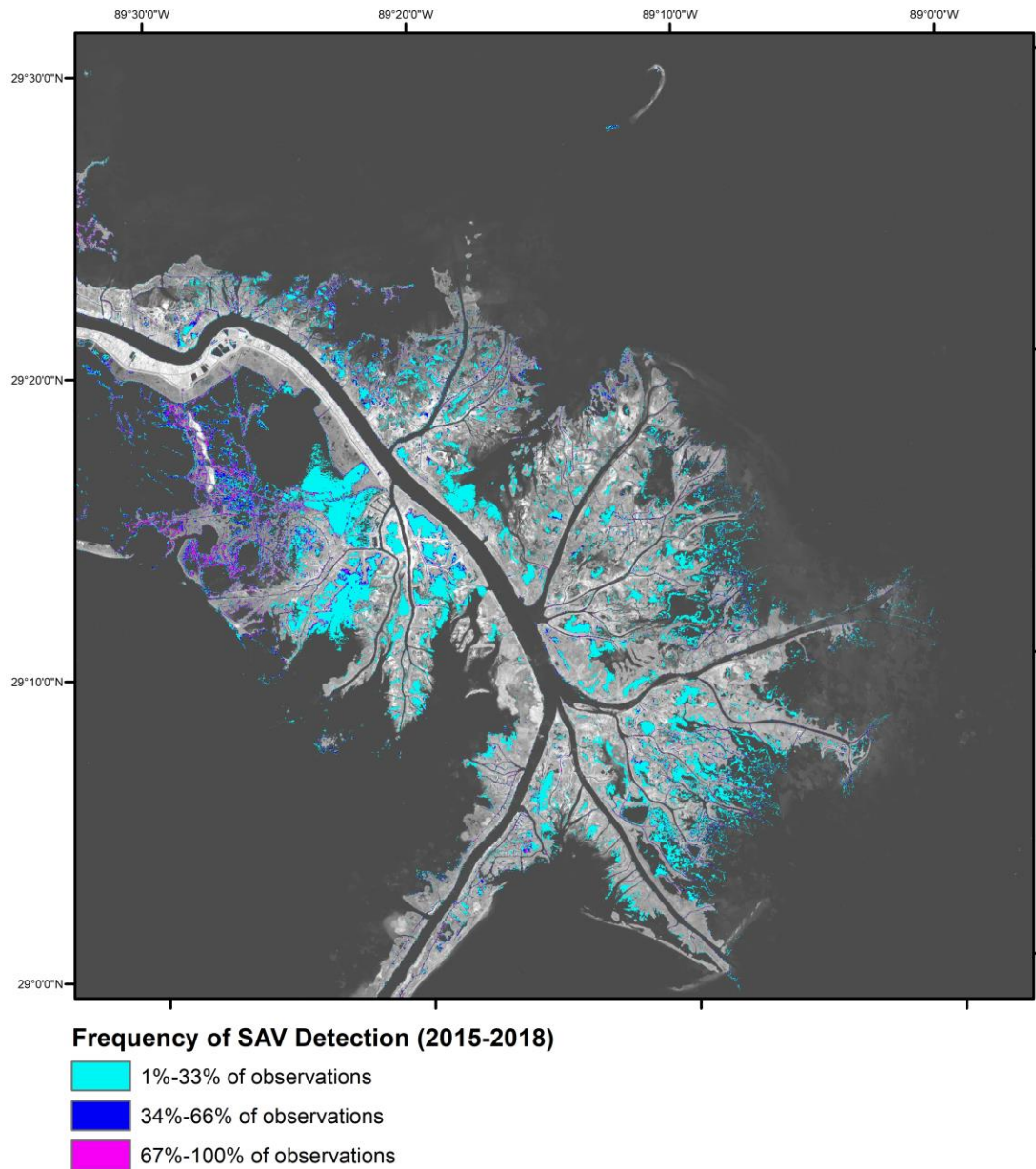- 67%-100% of observations

Figure A21. Visualization of the Frequency of SAV Detection layer in a 30'x30' cell from approximately 29.5°N to 29°N and 89.5°W to 89°W.